CLRC

Technical Report
RAL-TR-1999-023

# Hydrogenic Ionization Model for Mixtures in Non-LTE Plasmas

A Djaoui

8th April 1999

COUNCIL FOR THE CENTRAL LABORATORY OF THE RESEARCH COUNCILS

Enquiries about copyright, reproduction and requests for additional copies of this report should be addressed to:

The Central Laboratory of the Research Councils
Library and Information Services
Rutherford Appleton Laboratory
Chilton
Didcot
Oxfordshire
OX11 0QX
Tel: 01235 445384 Fax: 01235 446403
E-mail library@rl.ac.uk

**ISSN 1358-6254**

# HYDROGENIC IONIZATION MODEL FOR MIXTURES IN NON-LTE PLASMAS

A. Djaoui

*Central Laser Facility, Rutherford Appleton Laboratory, Chilton, Didcot, Oxon, OX11 0QX, U.K.*

**Abstract**

The Hydrogenic Ionization Model for Mixtures (HIMM) is a non-Local Thermodynamic Equilibrium (non-LTE), time-dependent ionization model for laser-produced plasmas containing mixtures of elements (species). In this version, both collisional and radiative rates are taken into account. An ionization distribution for each species which is consistent with the ambient electron density is obtained by use of an iterative procedure in a single calculation for all species. Energy levels for each shell having a given principal quantum number and for each ion stage of each species in the mixture are calculated using screening constants. Steady-state non-LTE as well as LTE solutions are also provided. The non-LTE rate equations converge to the LTE solution at sufficiently high densities or as the radiation temperature approaches the electron temperature. The model is particularly useful at low temperatures where convergence problems are usually encountered in our previous models. We apply our model to typical situation in x-ray laser research, laser-produced plasmas and inertial confinement fusion. Our results compare well with previously published results for a selenium plasma.

# 1 INTRODUCTION

The ionization state distribution of a plasma is a fundamental quantity which is required for the determination of the equation of state, thermal and electrical conductivities, radiative properties and the stopping power for fast charged particles. If the plasma is in Local Thermodynamic Equilibrium (LTE), the ionization depends only on local plasma conditions (density and temperature) and the excitation and ionization distribution of the plasma is determined by Fermi and Boltzmann statistics. Equilibrium occurs in a high density plasma where collisions dominate and/or in an optically thick plasma, where the radiation field is a Planckian at the local temperature. Low density and/or optically thin plasmas have often a charge state which is significantly lower than the equilibrium value. Radiative emission processes are not balanced by absorption since photons are able to escape from the plasma. In these non- LTE plasmas it is necessary to solve atomic rate equations describing the balance between excitation/de-excitation and ionization/recombination processes. If the plasma state (density and temperature) changes on a time scale which is faster than the time scale for atomic processes, a time-dependent solution of the non-LTE rate equations is then required.

Typically, all three situations (LTE, steady-state non-LTE and transient non-LTE) may be encountered during the interaction of a high power laser beam with a target. In the low density, high temperature blow-off region of laser-produced plasma, non-LTE usually applies. Heat conduction (electron thermal or radiative) from the laser deposition region deep into solid targets results in a high density region where LTE may apply. Short laser pulses create plasmas which evolve on a time scale much shorter than the time needed for ionization to come into steady-state equilibrium with time-dependent density and temperature. It is therefore desirable to have a single model which is applicable, with reasonable accuracy, to all situations encountered in current experiments.

The solution of the ionization problem is complicated because multi-electron ions can have an extremely large number of excited states, thus leading to rate equations that require the inversion of impractically large matrices. Atomic data is not always available for all quantum states which are important. This has led many authors to develop a variety of simpler models. In some models for K-shell spectroscopy[1–4] for example, the H-like, He-like and Li-like ionization stages are treated in detail while ionization stages between neutral and Be-like are treated with their ground states only. By gathering excited bound states and free states into one superlevel and then computing transitions between superlevels, a mixed model is constructed[5]. In the average atom model[6,7], average populations for bound electron shells with a given principal quantum number and the average ionization state of the plasma are calculated by using scaled hydrogenic rates. Level populations of ions having

a charge different from the average ion are, under certain approximations, estimated from the average populations. These approximations rely on a statistical method, such the binomial distribution[8–10]. More involved statistical methods have also been developed for estimating integer charge state distributions from any average atom model for LTE[11] and non-LTE[12] plasmas. Another method, the hybrid-atom model, assumes that excited level populations for ions in different charge states have a common characteristic given by the average atom model, and only the equations for the abundance of different charge states are solved[13]. The validity of different approximations is not always established and a more detailed model, which does not make any assumptions on the distribution of the excited states of a given ion, or the distribution around the average charge ion, is needed.

A more direct and accurate method for calculating the ionization distribution is described by Lee[14]. This also uses a scaled hydrogenic model but goes beyond the average atom model by treating each ionization state explicitly. In this work we extend Lee's model by giving an efficient method for the solution of the time-dependent equations in addition to the steady-state case. We also allow for more than one atomic species (element) in a given calculation. The model takes into account the ground state as well as the excited state for each ion, but only one energy level per principal quantum number is used. Electron impact ionization from excited states, which is known to be important, is taken into account. With the assumption that energy levels couple to the ground state of the next ionization stage only, the finite difference equations are cast into a tridiagonal form which is solved with minimum computational effort. The calculated electron density for a mixtures such as fused quartz ($SiO_2$) for example, is consistent with the states of ionization of both silicon and oxygen in the quartz. An LTE option is provided in order to allow a good description of cold solid targets as encountered in experiments and to test the high density limit of the non-LTE model. The resulting code, HIMM (Hydrogenic Ionization Model for Mixtures), is applied to typical problems in laser-plasma experiments and in x-ray laser research.

The scaled hydrogenic model gives qualitatively correct results for the ionization balance in most situations, but it has also some limitations. An average level treatment typically underestimates the excited state populations, and the rate of ionization from such states. For example, in the case of the Ne-like charge state, the ground state has a closed shell and the first excited state has many metastable levels[15,16]. The scaled hydrogenic model does not include any metastables and tends to underestimate the population of the first excited state. As a result, ionization from the Ne-like to the F-like charge state is underestimated.

Rates for photoionization and optical pumping of excited states by photon re-absorption can be taken into account in the model. In this version we limit

ourselves to Planckian fields, the radiation then being characterised by a temperature. Moreover, we assume that the electron distribution can well be approximated by one Maxwellian distribution, and no hot electron component is taken into account here.

We first describe the atomic model in section 2. We show a procedure for dealing with continuum lowering in the case of a mixture of different ionization states of different elements. The procedure for solving the time-dependent equation is presented in section 3. The excited state populations are expressed in terms of the ground state populations for which a tridiagonal system of equations is solved. In section 4, we compare our model to previously published calculations and present results which are relevant to current problems in x-ray laser research and short pulse target interaction experiments. We illustrate the application to a mixture by calculating an approximate ionization for fused quartz at solid density and compare the results with previous calculations. The effect of the radiation field inside a hohlraum on the ionization of a typical inertial confinement fusion capsule is illustrated. Finally, details of the rates used in this model are given in the appendix.

## 2 ATOMIC MODEL AND CONTINUUM LOWERING

A variety of prescriptions exist for the calculation of the ionization energy for a given level which differ in the way inner and outer screening are taken into account[8,17,18]. Here we use More's formula[17] which gives adequate accuracy for the purpose of this work. For each atomic species $j$ and each ionization stage $i$, energy levels are generated from screening constants[17]. Only the ground state and singly excited states are taken into account. The screened charge $Q_{jin}$ and the ionization energy $I_{jin}$ of species $j$ ionization stage $i$ and shell $n$ are given by

$$Q_{jin} = Z_j - \sum_{m<n} \sigma(n,m) M_{jim} - \frac{1}{2}\sigma(n,n)(M_{jin} - 1) \tag{1}$$

$$I_{jin} = E_n^0 - \frac{Q_{jin}^2 e^2}{2a_0 n^2} \tag{2}$$

where $Z_j$ is the atomic number of species $j$, $M_{jin}$ and $M_{jim}$ are the number of electrons (integer numbers) in the $n^{th}$ and $m^{th}$ shells respectively, of ion stage $i$. $a_0$ is the Bohr radius, $e$ the charge of the electron, while $\sigma(n,m)$ is the screening constant of shell $n$ per electron in shell $m$. $E_n^0$, the energy associated with outer screening is given by

$$E_n^0 = \frac{1}{2}\frac{e^2}{r_{jin}}\sigma(n,n)M_{jin} + \sum_{m>n}^{(nmax)_{ji}} \sigma(m,n)\frac{e^2 M_{jim}}{r_{jim}} \tag{3}$$

$$r_{jin} = \frac{a_0 n^2}{Q_{jin}} \tag{4}$$

The number of shells $(nmax)_{ji}$ depends on electron density and temperature when continuum lowering is included. Ground states of low-lying ionization stages may be pressure ionized thus making the number of ionization stages present in the plasma a function electron density and temperature. This necessitates an iterative solution when continuum lowering is included.

Continuum lowering may be taken into account using the modified Stewart and Pyatt formula[19]. This is necessary for metals such as aluminium, in order for the model to give a state of ionization consistent with the valence of the metal under normal conditions. The ionization potential depression in $eV$ is given by

$$\Delta E_{ji} = 2.16 \times 10^{-7} \frac{Z_{ji}}{R_j} \left( \left( 1 + \left( \frac{D}{R_j} \right)^3 \right)^{2/3} - \left( \frac{D}{R_j} \right)^2 \right) \tag{5}$$

where $Z_{ji}$ is the charge of the ion in question, $D$ is the Debye length for the mixture and $R_j$ the ion radius for species $j$ in $cm$. Following Cox and Giuli[20] we assume that if the electron density were uniform, the average volume occupied by element $j$ contains just $Z_j$ electrons. $R_j$ is then given by $(4\pi/3)R_j^3 N_e^* = Z_j$ where $N_e^*$ is the electron density in the case of complete ionization. This leads to

$$R_j = \left( \frac{3}{4\pi N_A \rho} \right)^{1/3} \frac{Z_j^{1/3} \langle A \rangle^{1/3}}{\langle Z \rangle^{1/3}} \tag{6}$$

where $N_A$ is Avogadro's number and $\rho$ the plasma density. We define the average $\langle y \rangle$ as an atom number fraction average: $\langle y \rangle = \sum f_j y_j$, where $f_j$ is the atomic fraction of species $j$. Note that Cox and Giuli[20] use a mass fraction average instead by defining a relative mass abundances $x_j$, where $x_j = A_j f_j / \langle A \rangle$.

The Debye length D for the mixture is given by $1/D^2 = 1/D_e^2 + \sum_j 1/D_j^2$ where $D_e$ is the Debye length for electrons and $D_j$ the Debye length for ions of species $j$ having an average ionization state $Z_j^*$. When electrons and ions have the same temperature, $D$ is given by

$$\frac{1}{D^2} = \frac{4\pi e^2 N_e}{kT} \left( 1 + \frac{\langle Z^{*2} \rangle}{\langle Z^* \rangle} \right) \tag{7}$$

With the use of Eqs. 3, 4 and 5, each ion stage of each element in the mixture, will have a different value for the corresponding continuum lowering, and therefore a number of states which depends on density and temperature.

## 3 IONIZATION DISTRIBUTION FOR A MIXTURE

*Time-dependent non-LTE model*

$N_{ji}(l)$, the population of each level $l$ (which corresponds to a shell with principal quantum number $n$), of ionization stage $i$ of species $j$ can be calculated from the solution of the following system of time-dependent rate equations, as given in Ref. [14].

$$\frac{dN_{ji}(l)}{dt} = -[W_{ji}^{pi}(l) + n_e R_{ji}(l)]N_{ji}(l) + S_{j(i+1)}(l)N_{j(i+1)}(1) - \sum_{k=1}^{K_{ji}} \tau_{ji}^{lk} N_{ji}(k) + \sum_{k=1}^{K_{j(i-1)}} \{[W_{j(i-1)}^{pi}(k) + n_e R_{j(i-1)}(k)]N_{j(i-1)}(k) - S_{ji}(k)N_{ji}(1)\}\delta_{l,1} \tag{8}$$

where

$$\tau_{ji}^{lk} = -n_e(C_{ji}^{kl})^e - (W_{ji}^{kl})^{pa}, \qquad l > k$$
$$\tau_{ji}^{lk} = -n_e(C_{ji}^{kl})^d - A_{ji}^{kl} - (W_{ji}^{kl})^{se}, \qquad l < k$$
$$\tau_{ji}^{ll} = \sum_{k<l}[n_e(C_{ji}^{lk})^d + A_{ji}^{lk} + (W_{ji}^{lk})^{se}] + \sum_{k>l}^{K_{ji}}[n_e(C_{ji}^{lk})^e + (W_{ji}^{lk})^{pa}]$$

$W_{ji}^{pi}(l)$ represents the photo-ionization rate (corrected for stimulated recombination), while $n_e R_{ji}(l)$ represents the total collisional ionization rate (direct and excitation-autoionization) from level $l$ of ion $i$. $S_{j(i+1)}(l)$ is the total recombination (collisional and radiative) rate into level $l$ of ion $i$ from the ground state of ion $(i+1)$.

$A_{ji}^{kl}$ is the spontaneous emission rate from level $k$ to level $l$. $(W_{ji}^{kl})^{pa}$ and $(W_{ji}^{kl})^{se}$ are the photo-absorption and stimulated emission rates between levels $l$ and $k$. $(C_{ji}^{kl})^e$ and $(C_{ji}^{kl})^d$ are the collisional excitation and de-excitation rates between levels $l$ and $k$.

$K_{ji}$ is the highest energy level of ion $i$ of species $j$ included in the calculation or allowed by continuum lowering. $\delta_{l,k}$, the Kronecker delta function, is unity if $l = k$ and zero otherwise. The electron density $n_e$, is the sum of contributions from all species

$$n_e = \sum_j Z_j^* f_j N_{at} = \sum_j Z_j^* N_j \tag{9}$$

where $N_{at}$ is the total atomic density.

The direct solution of the time-dependent rate equations for all species is complicated by the need to invert large matrices. There can also be large difference in rate coefficients leading to a stiff problem which requires an implicit method of solution. A better approach is to deal with each species separately (we therefore drop the species subscript $j$ for the rest of this sub-section) and to iterate for a self-consistent $n_e$, if necessary. Each species contributes to the free electron density according to Eq. 9. Iteration is required whenever continuum lowering is included and when the mass density or atomic densities are specified instead of electron density. With the assumption that energy levels couple to the ground state of the next ionization stage only[14], an efficient method of solution of the finite difference equations for each species is found. This assumption is valid when direct ionization from singly excited states dominates. Coupling to excited states of the next ionization stage can occur when inner shell excitation and ionization become significant[21]. Modeling of these processes would require detailed energy levels and cross-sections and results in much more complicated models than screened hydrogenic models.

First the excited states ($l \geq 2$ in Eq. 8) are expressed as

$$\frac{dN_i(l)}{dt} + \sum_{k=2}^{K_i} T_i^{lk} N_i(k) = S_{i+1}(l) N_{i+1}(1) - \tau_i^{l1} N_i(1) \qquad l,k \geq 2 \qquad (10)$$
$$T_i^{lk} = [W_i^{pi}(l) + n_e R_i(l)]\delta_{l,k} + \tau_i^{lk}$$

Starting with known quantities at time $t^{(n)}$, the calculation is advanced by a timestep $\Delta t$. By taking the implicit form of the finite difference equation, an expression for the excited state populations of ion $i$ at time $t^{(n+1)} = t^{(n)} + \Delta t$ is derived in terms of ground state populations of ions $i$ and $i+1$ at time $(n+1)$. By defining a new matrix $\tilde{T}_i^{lk}$ and writing the populations in terms of its inverse we obtain

$$\begin{aligned} N_i(k)^{(n+1)} = \sum_{l=2}^{L_i} [\tilde{T}_i^{-1}]^{kl} \{ & N_i(l)^{(n)} - \tau_i^{l1} \Delta t N_i(1)^{(n+1)} \\ & + S_{i+1}(l) \Delta t N_{i+1}(1)^{(n+1)} \} \\ \tilde{T}_i^{lk} = \delta_{l,k} + T_i^{lk} \Delta t & \end{aligned} \qquad (11)$$

where $L_i = K_i$, is the highest level of ion $i$.

Next the ground state equations ($l = 1$ in Eq. 8) can be written as

$$\begin{aligned} \frac{dN_i(1)}{dt} + [W_i^{pi}(1) + n_e R_i(1) + \tau_i^{11} + S_i(1) + \sum_{k=2}^{K_{i-1}} S_i(k)] N_i(1) \\ - [W_{i-1}^{pi}(1) + n_e R_{i-1}(1)] N_{i-1}(1) - S_{i+1}(1) N_{i+1}(1) \end{aligned}$$

$$= -\sum_{k=2}^{K_i} \tau_i^{1k} N_i(k) + \sum_{k=2}^{K_{i-1}} [W_{i-1}^{pi}(k) + n_e R_{i-1}(k)] N_{i-1}(k) \qquad (12)$$

Here the left hand side of the equal sign depends on ground state populations only, while the right hand side contains the dependence on excited states. By taking the implicit form of this equation and using equation 11 for the excited state populations a tridiagonal system of equations is obtained for the ground state populations, mainly

$$a_i N_{i-1}(1)^{(n+1)} + b_i N_i(1)^{(n+1)} + c_i N_{i+1}(1)^{(n+1)} = d_i \qquad (13)$$

where

$$\begin{aligned}
a_i &= -[W_{i-1}^{pi}(1) + n_e R_{i-1}(1)]\Delta t \\
&\quad + \sum_{k=2}^{K_{i-1}} [W_{i-1}^{pi}(k) + n_e R_{i-1}(k)]\Delta t \sum_{l=2}^{L_{i-1}} [\tilde{T}_{i-1}^{-1}]^{kl} \tau_{i-1}^{l1} \Delta t \\
b_i &= 1 + W_i^{pi}(1) + n_e R_i(1)\Delta t + \tau_i^{11}\Delta t + \sum_{k=1}^{K_{i-1}} S_i(k)\Delta t \\
&\quad - \sum_{k=2}^{K_i} \tau_i^{1k}\Delta t \sum_{l=2}^{L_i} [\tilde{T}_i^{-1}]^{kl} \tau_i^{l1}\Delta t \\
&\quad - \sum_{k=2}^{K_{i-1}} [W_{i-1}^{pi}(k) + n_e R_{i-1}(k)]\Delta t \sum_{l=2}^{L_{i-1}} [\tilde{T}_{i-1}^{-1}]^{kl} S_i(l)\Delta t] \\
c_i &= -S_{i+1}(1)\Delta t + \sum_{k=2}^{K_i} \tau_i^{1k}\Delta t \sum_{l=2}^{L_i} [\tilde{T}_i^{-1}]^{kl} S_{i+1}(l)\Delta t \\
d_i &= N_i(1)^{(n)} - \sum_{k=2}^{K_i} \tau_i^{1k}\Delta t \sum_{l=2}^{L_i} [\tilde{T}_i^{-1}]^{kl} N_i(l)^{(n)} \\
&\quad + \sum_{k=2}^{K_{i-1}} [W_{i-1}^{pi}(k) + n_e R_{i-1}(k)]\Delta t \sum_{l=2}^{L_{i-1}} [\tilde{T}_{i-1}^{-1}]^{kl} N_{i-1}(l)^{(n)}
\end{aligned}$$

Eqs. 9, 11 and 13 are iterated until convergence of $Z_j^*$ of each species in the mixture. An 'inner' iteration loop for continuum lowering, is also performed for every 'outer' iteration on $Z_j^*$. The iterative procedure is defined by relating the electron density 'guess' $n_g^{(i+1)}$ for iteration $(i+1)$, to three previous estimates as obtained after iterations $(i)$, $(i-1)$ and $(i-2)$, mainly

$$n_g^{(i+1)} = \lambda n_e^{(i)} + \tfrac{1}{2}(1-\lambda) n_e^{(i-1)} + \tfrac{1}{2}(1-\lambda) n_e^{(i-2)}$$

where $0 < \lambda < 1$. A value $\lambda = 0.5$ is usually used. The procedure is robust and has proved to be reliable even at very low temperatures, where convergence problems are normally encountered with some other methods. Most cases considered converge in ten to twenty iterations.

*Steady-state non-LTE model*

The steady-state solution which is also derived by Lee[14] is given next. In steady state equilibrium, The increase of the ground state of an ionization stage by ionization is exactly equal to its decrease by recombination into a level of the next lower ionization stage. The last term in Eq. 8, which included the Kroenecker delta, is therefore zero. By also setting $dN_{ji}(l)/dt$ to zero for every level, the equation reduces to

$$\sum_{k=1}^{K_{ji}}(T_{ji}^{lk})N_{ji}(k) = S_{j(i+1)}(l)N_{j(i+1)}(1) \tag{14}$$

where

$$T_{ji}^{lk} = [W_{ji}^{pi}(l) + n_e R_{ji}(l)]\delta_{l,k} + \tau_{ji}^{lk} \tag{15}$$

By writting the level population in terms of the inverse of the matrix T and the ground state of the next ionization stage,

$$N_{ji}(k) = \sum_{l=1}^{L_{ji}}[T_{ji}^{-1}]^{kl}S_{j(i+1)}(l)N_{j(i+1)}(1). \tag{16}$$

The total ionization rate of the ith ion stage can be written as $\alpha_{ji}N_{j(i+1)}(1)$,while the total recombination rate of the (i+1) stage can be written as $\beta_{j(i+1)}N_{j(i+2)}(1)$, where

$$\alpha_{ji} = \sum_{k}^{K_{ji}}[W_{ji}^{pi}(k) + n_e R_{ji}(k)]\sum_{l}^{L_{ji}}[T_{ji}^{-1}]^{kl}S_{j(i+1)}(l)$$

$$\beta_{j(i+1)} = \sum_{k}^{K_{ji}} S_{j(i+1)}(k) \sum_{l}^{L_{j(i+1)}} [T_{j(i+1)}^{-1}]^{1l}S_{j(i+2)}(l).$$

At steady state the total ionization rate of the ith stage is exactly balanced by the total recombination of the (i+1) ion stage. We then have

$$\alpha_{ji}N_{j(i+1)}(1) = \beta_{j(i+1)}N_{j(i+2)}(1), \qquad 1 \le i \le Z_j - 1.$$

The solution proceeds differently from the time dependent case. Using the above recursive relation, the fully ionized (or highest ionization stage) fraction of species $j$ is calculated first from

$$\frac{N_{Z_j+1}}{N_j} = \frac{1}{1 + \sum_{ilk}[T_{ji}^{-1}]^{lk}S_{j(i+1)}(k)(\beta_{j(i+1)}/\alpha_{ji})(\beta_{j(i+2)}/\alpha_{j(i+1)})\ldots(\beta_{jZ_j}/\alpha_{j(Z_j-1)})}$$

Ground state populations of lower ionization stages are obtained from the recursive formula and the excited states from Eq. 16.

We have checked that the steady state solution is reproduced by the time-dependent equations for long enough times, no matter what the initial conditions are. Both time-dependent (for sufficiently long times) and steady state equations reproduce the LTE ionization distribution at sufficiently high densities.

*LTE model*

For completeness, the LTE solution which can also be found in Mihalas[22] is given here. In LTE, Eq. 16 for the excited state populations reduces to the well known Saha-Boltzmann equation

$$N_{ji}(k) = n_e \Phi_{ji}(k) N_{j(i+1)}(1) \tag{17}$$

where

$$n_e \Phi_{ji}(k) = n_e \frac{g_{ji}(k)}{g_{j(i+1)}(1)} \frac{1}{2} \left(\frac{h^2}{2\pi m k T}\right)^{3/2} e^{-(I_{jik}+\Delta E_{ji})/kT}$$

The highest ionization stage (fully ionized) fraction of species $j$ is given by

$$\frac{N_{Z_j+1}}{N_j} = \frac{1}{1 + \sum_{ik} n_e \Phi_{ji}(k) \{ n_e \Phi_{j(i+1)}(1) n_e \Phi_{j(i+2)}(1) \ldots n_e \Phi_{j Z_j}(1) \}}$$

By applying Eq. 17, ground and excited state populations of lower ionization statges can then be calculated.

## 4 RESULTS

*Comparisons*

In Fig. 1, we compare the non-LTE results from our model to Lee's[14] for a selenium plasma in steady-state and at a fixed electron density and temperature. Both codes predict the dominance for the Neon-like ionization stage. The small difference between the codes is the result of differences in rate coefficients.

In Fig. 2 we make a further comparison with a completely different collisional radiative model[16], were particular attention is paid to dielectronic recombination and excitation-autoionization rates. The charge state fraction of the fluorine-like, neon-like and sodium-like selenium are plotted as a function of temperature at a fixed ion density. The dashed curve corresponds to Osterheld's[16] average level calculation. The agreement is also good and the small differences are the result of differences in rate coefficients and possibly energy levels.

*Application to x-ray laser plasmas*

Accurate rate coefficients for various processes and various ions are needed for understanding the ionization balance of laboratory and astrophysical plasmas in general. In x-ray laser research, both neon-like and nickel-like scheme are currently the subject of intense investigations. For the neon-like scheme the importance of various atomic processes in determining the ionization balance can be seen in Fig. 3. The full curve includes all ionization and recombination process while the dashed curves shows the effect of switching off either collisional excitation, radiative recombination, or dielectronic recombination. This shows that, for these conditions, while radiative recombination is unimportant, collisional excitation and dielectronic recombination have a substantial effect on the ionization balance.

In calculating the ionization balance for the nickel-like x-ray laser scheme, it is necessary to take into account excitation-autoionization (EA) in addition to collisional ionization (CI) and dielectronic recombination (DR). Our model includes EA rates for the zinc-like and copper-like isoelectronic sequences for elements with $34 \leq Z \leq 92$. The effect of these rates on the Ni-like fraction for tungsten at a fixed ion density and different temperatures is shown in Fig. 4. When no DR or EA are taken into account the Ni-like fraction peaks at a temperature of about 2000 eV. Adding DR rates results in a large shift of the peak to about 5000 eV. Further adding EA rates for Cu-like and Zn-like ions shifts the peak of Ni-like fraction back to about 2000 eV. However it should be noted that the effect of EA is not simply to cancel DR, since as the figure shows, not only does the peak of the curves shift, the magnitude of the peak as well as the shape of the curves change, when both DR and EA are added to CI.

*Time-dependence*

It has long been known that, in x-ray laser research[9,15,23] that uses high power lasers, the ionization balance can be far from steady-state equilibrium. The interaction of a laser beam with a target results in a rapidly evolving plasma where the time scale for ionization is usually longer than the pulse length or the timescale for hydrodynamic changes. The use of double-pulses, the first to create a uniform plasma, and a second, short pulse, to ionize it to the required stage[24], has made time-dependent effects even more important. Here we illustrate our model by showing time-dependent ionization, relevant to x-ray lasers, at fixed ion density when the temperature jumps from an initial low temperature to a high temperature. Figure 5 shows the case for selenium for three ion densities and two temperatures while Fig. 6 shows the case for tungsten. For the same temperature (Te=1000 eV), both Se and W relax to steady-state in approximately the same time. This relaxation time increases from about 10 ps to more than 300 ps as the ion density decreases

from $10^{21} cm^{-3}$ to $10^{19} cm^{-3}$. In the case for tungsten, the Ni-like stage is only reached at the highest densities and temperatures shown. Laser energy is normally deposited near the point where $n_i = 10^{20} cm^{-3}$, but both lower and higher densities are rapidly heated by electron conduction. The timescale for ionization increases as the density decreases (or as the plasma expands). A realistic calculation would requires space and time-dependent information about the density-temperature history of the plasma. This requires a complex simulation[9] where hydrodynamics and atomic physics of ionization are coupled and advanced in time simultaneously.

*LTE versus non-LTE*

Laser target interaction experiments produce plasmas with a wide range of densities and temperatures. At one extreme is a high temperature low density region, while at the other, a low temperature shock compressed matter. It is therefore desirable to have a model which describes the non-LTE situation in the low density region but reduces to LTE in the high density region. In Fig. 7 we show the ionization of aluminium as function of mass density at a fixed temperature. At the lowest densities, the difference between the LTE and non-LTE ionization is of the order of a factor of two. For densities greater than $0.1 g cm^{-3}$ the non-LTE ionization progressively reduces to the LTE value. For these high densities continuum lowering changes the ionization significantly. The irregularity shown at about $0.3 g/cm^2$ is the result of pressure ionization of excited states of F-like aluminium as density increases. The large discontinuity at at about $3 g/cm^2$ corresponds to the pressure ionization of Na-like aluminium (ie removal of the ground state into the continuum) as the density increases. These features are absent when continuum lowering is switched off. The picture depicted in Fig. 7 is quite common in laser-produced plasmas and shows that departure from LTE should be taken into account when modelling equation of state, and radiative properties of these plasmas.

*Mixtures*

A new feature in our model is the ability to treat many atomic species in a plasma in one single calculation. The calculated ionization of each species is then consistent with the ambient electron density in the plasma. We apply our model here, to some recent experiments, where the ionization front driven by a high intensity ultra-short laser pulse irradiation of a transparent medium ($SiO_2$), was seen to move supersonically[25,26]. In order to simulate the experiment a knowledge of the degree of ionization near solid density is needed. Fig. 8 shows the ionization of $SiO_2$ as a function of temperature and at solid density. No continuum lowering is included in these calculations. Both LTE and non-LTE models yield practically the same result at this density. The experiments however, probe a region where the ionization is very low ($< 0.1$) and where the temperature is also expected to be of the order of one eV. Fig.

9 shows the same result as Fig. 8, but on a log-log scale. We have also plotted the results from an approximate method[25] for comparison. In our model the first ionization energy is 13.6 eV for oxygen and 8.1 eV for silicon and only when the temperature is a few eV that substantial ionization ($> 0.01$) is obtained. The approximate method treats the ionization energies as a continuous function of charge state[25] with charge states near neutral having much lower ionization energies. This leads to higher ionization at the lowest temperatures as compared to our model. We note that an improvement to our model can be obtained by use of band gap energies for solid $SiO_2$ instead of isolated atoms ionization potentials.

*Effect of radiation field*

In the non-LTE cases presented so-far, no radiation field was taken into account. Neglect of radiative rates is valid when the plasma is optically thin to all photons. This is no longer the case if an external radiation field (in addition to the plasma self emission) is present. Such situation occurs in a capsule as used inside a hohlraum in indirect drive inertial confinement fusion experiments. The outside of the capsule is made of brominated plastic (CH with 0.25% Br and 5% O) shell which is heated with x-rays fom the wall of the hohlraum. The x-rays penetrate through the ablated material and are deposited in the plastic shell. The opacity of the heated material has then a direct effect on the penetration depth of the x-rays and possibly on the performance of the capsule. Figure 10 shows typical density-temperature conditions as well as the ionization state of the plasma when no radiation is taken into account. Although the non-LTE ionization for Br is quite different to the LTE value the average values in the plasma (C, H, Br and O) are similar. The low atomic number elements (C, H, and O) in the mixtures are in practically in LTE at the electron density considered, while the higher atomic number Br is far from LTE when no radiation is taken into account. The effect of including a radiation field is shown in Fig. 11. As the radiation temperature approaches the electron temperature the ionization of Br tends towards LTE. This partly justifies the use of LTE opacities in previous simulation of these ICF capsules. It should be noted however that a more detailed simulation should solve the radiative transfer equation for a local photon spectrum, which should then be used for calculating radiative rates at each point in the plasma.

## 5 SUMMARY

A general ionization model for laser produced plasmas which is applicable over a wide range of temperatures and densities is presented. The model is particularly useful at low temperatures where convergence problems are usually encountered. Both LTE and non-LTE equations are solved. The model allows

for more than one atomic species, as encountered in many laser-produced plasmas. Energy levels for each shell (having a given principal quantum number), of each ion stage and of each species, are calculated using screening constants. Screened hydrogenic rates are used for most atomic processes. Excitation-autoionization rates are included for Cu-like and Zn-like ions. The model calculates the ionization distribution of each species that is consistent with the ambient electron density using an iterative procedure.

The results for a selenium plasma compare well with previously published calculations. Excitation-autoionization is shown to have a drastic effect on the Ni-like ion fraction in a tungsten plasma. Relaxation of a selenium and of a tungsten plasma towards steady-state, when instantaneously heated to keV temperatures, is shown to be strongly density-dependent. At the highest ion density shown these times are about 30 ps and increase as the density decreases.

Similar results are obtained from the non-LTE and LTE solutions at high densities. This is particularly the case for solid low temperature targets which are increasingly used in pump-probe experiments using short pulse lasers. By switching the continuum-lowering off, the model is capable of calculating ionization in insulators at temperatures of the order of 1 eV. The accuracy of such calculations can be improved by using the band gap energy instead of the ionization energy for the isolated ion.

## 6 ACKNOWLEDGEMENT

The author would like to thank Mr Richard Williams for his help in setting up the equations using Latex.

## APPENDIX A: RATE COEFFICIENTS

*CGS units are used except for the temperatures (kT) and energies which are expressed in eV.*

### Collisional rates

Most of the rates of atomic processes are calculated within the scaled hydrogenic approximation. **Collisional excitation** rates are taken from Post[7], where

$$n_e(C^{kl})^e = n_e \times 1.578 \times 10^{-5} \frac{f_{kl} e^{-x_{kl}}}{(kT)^{1/2} \Delta E_{kl}} G_{kl} M_k$$

$G_{kl}$ being the Gaunt factor and is given by

$$x_{kl} = \frac{\Delta E_{kl}}{kT}$$

$$G_{kl} = 0.19 \left[ 1 + 0.9 \left( \frac{l(l-k)}{20} \left( 1 - \left( 1 - \frac{2}{Z} \right) x_{kl} \right) \right) e^{x_{kl}} E_1(x_{kl}) \right]$$

Another choice for collisional excitation is taken from Sampson and Golden[27]. In this case

$$n_e(C^{kl})^e = n_e \times 4.356 \times 10^{-6} \frac{f_{kl} e^{-x_{kl}}}{(kT)^{1/2} \Delta E_{kl}} G'_{kl} M_k$$

where

$$G'_{kl} = e^{x_{kl}} \{ E_1(x_{kl}) + (1 - \frac{1.05}{Z}) k^{0.7} (\frac{\Delta E_{kl}}{I_k})^{0.6} x_{kl} E_{1.5}(x_{kl}) + H_k \left[ (\frac{\Delta E_{kl}}{I_k})^{r_k} + A_k (\frac{\Delta E_{kl}}{I_k} - 1) \right] E_2(x_{kl}) \}$$

$I_k$ is the ionisation energy and $E_p(x_{kl})$ is the $p^{th}$ exponential integral[28]. The constants H, A and r are given for k=1 to 10 in the following table.

| k | 1 | 2 | 3 | 4 | 5 | 6 | 7 | 8 | 9 | 10 |
|---|---|---|---|---|---|---|---|---|---|---|
| $H_k$ | 1.48 | 3.64 | 5.93 | 8.32 | 2.15k | 2.15k | 2.15k | 2.15k | 2.15k | 2.15k |
| $A_k$ | 1.30 | 0.59 | 0.38 | 0.286 | 0.229 | 0.192 | 0.164 | 0.141 | 0.121 | 0.105 |
| $r_k$ | 1.83 | 1.60 | 1.53 | 1.495 | 1.475 | 1.46 | 1.45 | 1.45 | 1.46 | 1.47 |

The **de-excitation** rates are calculated from detailed balance as

$$n_e \left( C^{lk} \right)^d = \frac{g(k)}{g(l)} e^{x_{kl}} n_e \left( C^{kl} \right)^e .$$

The Lotz formula[29] is used for the rate of **collisional ionization**

$$n_e\, R_i^{ci}\ (l) = n_e \times 6 \times 10^{-8} \xi_l^{1/2} \left(\frac{I_H}{I_l}\right)^{3/2}\ E_1\,(\xi_l)\, M_l$$

where $I_H = 13.6eV$ and $\xi_l = \frac{I_l}{kT}$.

The **3 body recombination** rates are derived again from detailed balance as follows,

$$S_{i+1}^{3b}\,(l) = \left[\frac{N_i(l)}{N_{i+1}(1)}\right]^*\ n_e\, R_i^{ci}(l)$$

where $*$ denotes the LTE value and is given by

$$\left[\frac{N_i(l)}{N_{i+1}(1)}\right]^* = n_e \frac{1.66 \times 10^{-22}}{(kT)^{3/2}}\ \frac{g_i(l)}{g_{i+1}(1)}\, e^{\xi_l}.$$

**Radiative rates**

The radiative **spontaneous emission** rates and corresponding oscillator strengths are calculated using hydrogenic formulae [7].

$$A^{lk} = 4.34 \times 10^7\ \frac{g(k)}{g(l)}\ \Delta E_{kl}^2\ f_{kl}\ M_k$$

In the case of a Planckian radiation field (with radiation temperature $kT_r$), the **photoabsorption** $(pa)$ and **stimulated emission** $(se)$ rates are given by

$$\left(W^{kl}\right)^{pa} = 4.34 \times 10^7\ \Delta E_{kl}^2\ f_{kl} \frac{M_k}{e^{\Delta E_{kl}/kT_r} - 1}$$

$$\left(W^{lk}\right)^{se} = 4.34 \times 10^7\ \frac{g(k)}{g(l)}\ \Delta E_{kl}^2\ f_{kl} \frac{M_k}{e^{\Delta E_{kl}/kT_r} - 1}$$

It can easily be shown that in LTE the rate of photoabsorption from level $k$ to $l$ is exactly balanced by the rate of spontaneous and stimulated emissions from level$l$ to $k$ ie..

$$N^*(k)\ \left(W^{kl}\right)^{pa} = N^*(l)\left[A^{lk} + (W^{lk})^{se}\right]$$

The spontanous **radiative recombination** rate does not depent on the presence of a radiation field and is given by

$$W_{i+1}^{rr}(l) = \left[\frac{N_i(l)}{N_{i+1}(1)}\right]^*\ \times 1.149 \times 10^7\ \frac{I_l^{5/2}}{Q}\ E_1(\xi_l)\ M_l$$

For a Planckian radiation field the **photo-ionization** ($pi$) rate is taken from Mihalas[22]

$$W_i^{pi}(l) \;=\; 2.28 \times 10^{-4} \;\frac{I_l^{5/2}}{Q} \int\limits_{I_l}^{\infty} dE \;\frac{J(E)}{E^4} \;\; M_l$$

Where Q is the effective charge of the ion and for a planckian radiation field with a temperature $kT_r$ $J(E)$ in $ergs/cm^2/s/eV$ is given by

$$J(E) \;=\; 5.04 \times 10^{10} \;\frac{E^3}{e^{E/kT_r} - 1}$$

The **stimulated recombination** ($sr$)rate

$$W_{i+1}^{sr}(l) \;=\; \left[\frac{N_i(l)}{N_{i+1}(1)}\right]^{\star} \;\times 2.28 \times 10^{-4} \;\frac{I_l^{5/2}}{Q} \int\limits_{I_l}^{\infty} dE \;\frac{J(E)}{E^4} \;\; e^{-E/kT} \;\; M_l$$

In the above equations, the photon energy intergrals are performed numerically using Romberg's method, which performs a change of valuable from E to $(1/E)$, thus mapping the infinite range of intergration into a finite one.

In LTE, photo-ionization is balanced by radiative spontaneous and stimulated recombination. ie

$$N_i^{\star}(l) \;\; W_i^{pi}(l) \;=\; N_{i+1}^{*}(1) \;\left[W_{i+1}^{sr}(l) \;+\; W_{i+1}^{rr}\,(l)\right]$$

**Processes involving doubly excited states**

The **dielectronic recombination** (DR) rates are given by Post[7]. Here we assume all recombination is to the ground state (l=1)

$$S_{i+1}^{DR}\,(1) \;=\; 2.4 \times 10^{-9}\; n_e \;\frac{B(Q)D(Q,kT)}{(kT)^{3/2}} \;\sum_k f_{1k}\; A(y) e^{-\bar{E}/kT} M_1$$

$$B(Q) \;=\; Q^{1/2}\,(Q+1)^{5/2} \;\;(Q^2+13.4)^{-1}$$

$$\frac{\bar{E}}{kT} \;=\; (Q+1)^2\;\Delta E_{1k}\,/(0.0735\;a\;kT)$$

$$a \;=\; 1 + \;0.015\;Q^3\,/\,(Q+1)^2$$

$$n_t^7 \;=\; 1.5084 \times 10^{17}\;Q^6\,(kT)^{1/2}\,/n_e$$

$M_1$ being the occupation of the ground state of the recombining ion.

For $\Delta n \neq 0$

$$A(y) = 0.5 \times y^{1/2} / (1 + 0.21y + 0.03y^2)$$

$$D(Q, kT) = \frac{0.0015 \left[(Q+1)\, n_t\right]^2}{1 + 0.0015 \left[(Q+1)\, n_t\right]^2}$$

For $\Delta n = 0$

$$A(y) = y^{1/2}/(1 + 0.105\, y + 0.015\, y^2)$$

$$D(Q, kT) = \frac{n_t/200}{1 + n_t/200}$$

We also include **excitation-autoionization** for the Cu-like[30] and Zn-like[31] ions for elements with $34 \leq Z \leq 92$. This last process is found to drastically alter the ionization distribution near the Ni-like stage.

The reverse processes for excitation-autoionization and dielectronic recombination are not included explicitly. In order for the model to recover the LTE value in the high density limit, the following ad-hoc procedure is used. The excitation-autoionization is added to direct ionization and the three body recombination calculated from the sum. In the dielectronic recombination formula, the oscillator strengths in the summation over excited states are multiplied by (1-(Radiative rate up)/(radiative rate down)). This has the desirable feature of reducing dielectronic recombination to zero as the radiation tempertaure approaches the electron temperature. The above procedure for dealing with doubly excited states is approximate and substantial work remains in this area.

## APPENDIX B: INPUT AND OUTPUT

HIMM read its input data from file 'himm.dat' which is attached to fortran stream 5 in the fortran source code using and 'open' statement. The name can be changed, but the code will have to be recompiled (in double precision) for the change to take effect. Here it is assumed that the input data file resides in the same directory as the executable code. An example input data file is shown next

```
Title: example CH
$newdata
nspec=2,
rho(1)=2.6e-6,
iatomz(1)=6, iatomz(2)=1,
atoma(1)=12., atoma(2)=1.,
atomfrac(1)=.5, atomfrac(2)=.5,
aspomul(1)=1., aspomul(2)=1.,
colemul(1)=1., colemul(2)=1.,
colimul(1)=1., colimul(2)=1.,
radrmul(1)=1., radrmul(2)=1.,
diermul(1)=1., diermul(2)=1.,
excamul(1)=1., excamul(2)=1.,
dense(1)=1.e18,
densi(1)=1.e18,
ndens=2, tdens=1.1,
ntemp=2, ttempe=1.4142,
tempe(1)=2.5e0,
fradte=1.0,
iforward=2, mode=3, lte=0,
mode2=3, tstep=1.e-12, nprstep=10,
iscl=0,
$end
2
0.   1.   0.   0.   0.   2.6e-6
3.e-11   10.   0.   0.   0.   2.6e-6
```

The first line of the input data contains a title. This is followed by most of the input data parameters in a namelist (between $newdata and $end). if 'iforward' equals 1 or 2, further data is read after the $end line according to the following fortran code

```
c       if(iforward.eq.1 .or.iforward.eq.2)then
c       read(5,*)ntime
c       do 50 itime=1,ntime
```

```
c       read(5,*)time(itime),tempe(itime),trad(itime),dense(itime)
c      & densi(itime),rho(itime)
c50     continue
c       endif
```

An explanation of input variables is given in table 1:

The main output is written to fortran stream 6 in file 'himm.out'. Table 2 shows some output which was produced by running the code with the example data file above.

Some additional files which present the results in a convenient form for plotting are also produced with each run. The number of files produced depends on the details of each run. Each case produced files on streams 30, 31 etc ... according to the following fortran statements.

```
c       write(30,88010)time(1),tempel,tradl,densel,densil,rhol,
c      & zbar,(zstar(k1),k1=1,nspec)
c       do 32 k1=1,nspec
c       write(30+k1,88014)time(1),tempel,tradl,densel,densil,rhol,
c      & zstar(k1),(fioniz(k1,kf1),kf1=1,iatomz(k1)+1)
c32     continue
c88010 format(1x,15(1pe9.2))
c88014 format(1x,110(1pe9.2))
```

When iforward is 0 or 1, the ionization distribution for each ground and excited state is also written on streams 41, 42 etc... according to the fortran statements below. The number of files produced depends on the input data.

```
c       kout40=40
c       do 207 k1=1,nspec
c       kout40=kout40+1
c      write(kout40,88096)iatomz(k1),tempel,tradl,densel,densil,rhol
c88096 format(1x,'Ztempeltradldenseldensilrhol',i4,5(1pe9.2))
c       do 107 iz=1,iatomz(k1)+1
c       write(kout40,88097)iz,fioniz(k1,iz),
c      & (fion(k1,iz,n1),n1=1,navmax)
c107    continue
c207    continue
c88097 format(1x,i4,15(1pe9.2))
```

## References


[1] Colombant, D. G. , Whitney, K. G. And Tidman, D. A., *The Physics of Fluids*, **18**, 1787 (1975)

[2] Duston, D. and Davis, *J., Phys. Rev. A*, **21**, 1664 (1980)

[3] Lee, R.W., Witten, B.L. and Stout, R.E., *J. Quantj. Spectrosc. Radiat. Transfer*, **32**, 91 (1984)

[4] Perusse, O., *Phys. Fluids B*, 4, 2007, (1992)

[5] Busquet, M., *Phys. Rev. A*, **25**, 2302, (1982)

[6] Lokke, W. A. and Grasberger, W. H., XSNQ-U: A Non-LTE Emission and Absorption Coefficient Subroutine, UCRL-52276 (1977)

[7] Post, D.E., Jensen, R. V., Tarter, C. B., Grasberger, W. H. And Lokke, W. A., *At. Data and Nucl. Tables*, **20**, 397 (1977)

[8] Mayer, S. Methods of opacity calculations, Unpublished Rep. LA-647, Los Alamos Scientific Laboratory, March, 1948.

[9] Djaoui, A. and Rose S. J., *J. Phys. B: At. Mol. Opt. Phys.*, **25**, 2745 (1992)

[10] Förster, A., Kahlbaum, T. and Rickert, A., *Supplement to Z. Phys. D - Atoms, Molecules and Clusters* **21**, 171 (1991)

[11] Faussurier, G., Blancard, C. and Decoster, A., *Phys. Rev. E* **56**, 3474 (1997)

[12] Dallot, P., Faussurier, G. and Decoster, A. *Phys. Rev. E* **57**, 1017 (1998)

[13] Itoh, M., Yabe, T. and Kiyokawa, S., *Phys. Rev. A*, **35**, 233 (1987)

[14] Lee, Y. T., *J. Quant. Spectrosc. Radiat. Transfer*, **38**, 131 (1987)

[15] Witten, B. L., London, R. A., and Walling, R. S., *Journal of the Optical Society of America B*, **5**, 2537 (1998)

[16] Osterheld A. L., Young B. K. F., Walling R. S., Goldstein W. H., Scofield J. H., Chen M., Shimkaveg G., Carter M., Shepherd R., MacGowan B. J., Da Silva L., Matthews D., Maxon S., London R. and Stewart R. E., Proceedings of Int. Colloquium on X-ray Lasers, Schliersee, Germany, Inst. Phys. Conf. Ser. No 125: pp 309-314, (1992)

[17] More R. M., *J. Quant. Spectrosc. Radiat. Transfer*, **27**, 345 (1982)

[18] Marchand, R., Caill, S., Lee, Y. T, *J. Quant. Spectrosc. Radiat. Transfer*, **43**, 149 (1990)

[19] More, R. M., Atomic physics in inertial confinement fusion, Applied Atomic Collision Physics, **2**, Academic Press, New York (1982)

[20] Cox J. P. and Giuli R. T. *Principles of Stellar Atmospheres* Gordon and Breach, New York, pp. 337-338, (1968)

[21] Henry, R.J.W. *Phys. Rep.* **68**, 1, (1981)

[22] Mihalas D., *Stellar Atmospheres*, Freeman, San Fransisco, CA, p. 114 (1978)

[23] Holden, P. B., Healy, S. B., Lightbody, M. T. M., Pert, G. J., Kingston, A. Robertson, A., Lewis, C. L. S., and Neely, D., *J. Phys. B: At. Mol. Opt. Phys.*, **27**, 341 (1994)

[24] Zhang, J., MacPhee, A. G., Lin, J., Wolfrum, E., Smith, R., Danson, C., Key, M. H., Lewis, C. L. S., Neely, D., Nilsen, J., Pert, G. J., Tallents, G. J., and Wark, J. S., *Science*, **276**, 1097 (1997)

[25] Vu, B.-T. V., Landen, O, L., and Szoke, A., *Phys. Plasmas*, **2**, 476 (1995)

[26] Ditmire, T., Gumbrell, E. T., Smith, R. A., Moutford, L., and Hutchinson, M. H. R., *Phys. Rev. Lett.*, **77**, 498 (1996)

[27] Sampson, D. H. and Golden, L. B. *Astrophys. J.*, **170**, 169 (1971) and Golden L. B. and Sampson D.H. *Astrophys. J.*, **163**, 405 (1971)

[28] Pagura V.I *Tables of the Exponential Integrals*, trans. D.G. Fry (New York: Pergamon Press) (1961)

[29] Lotz, W., *Astrophys. J. Suppl.*, **14**, 207 (1967); Z. Phys. **216**, 241 (1968)

[30] Mitnik, D., Mandelbaum, P., Shwob, J. L., Bar-Shalom, A., Oreg, J., and Godlstein, W. H., *Phys. Rev. A*, **53**, 3178 (1996)

[31] Mitnik, D., Mandelbaum, P., Shwob, J. L., Bar-Shalom, A., and Oreg, *J., Phys. Rev. A*, **55**, 307 (1997)

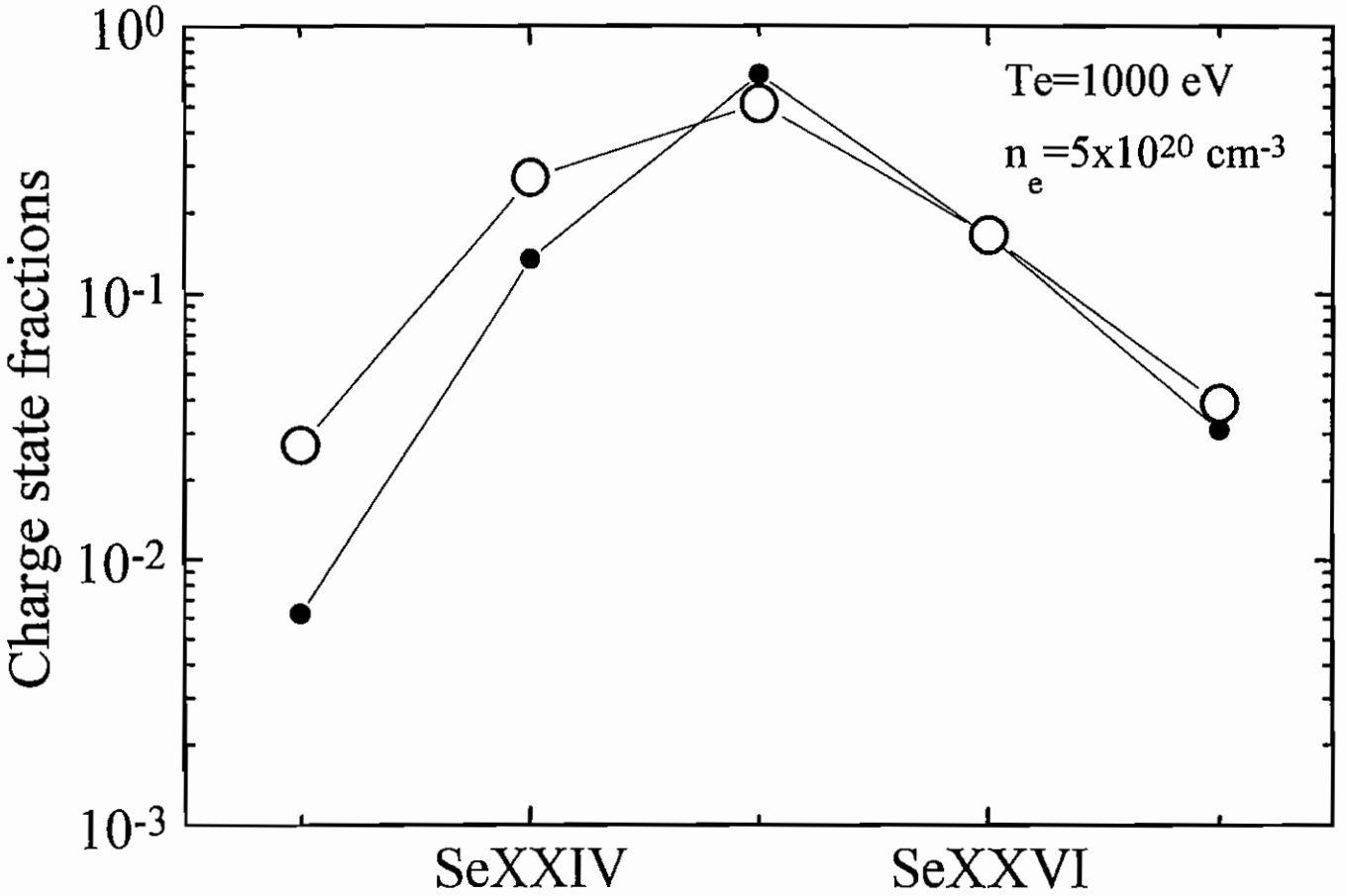


Fig. 1. Steady state charge state fractions in a selenium plasma at a fixed electron density and temperature. The empty circles are taken from Lee's work[14], while the dots are the results from our model.

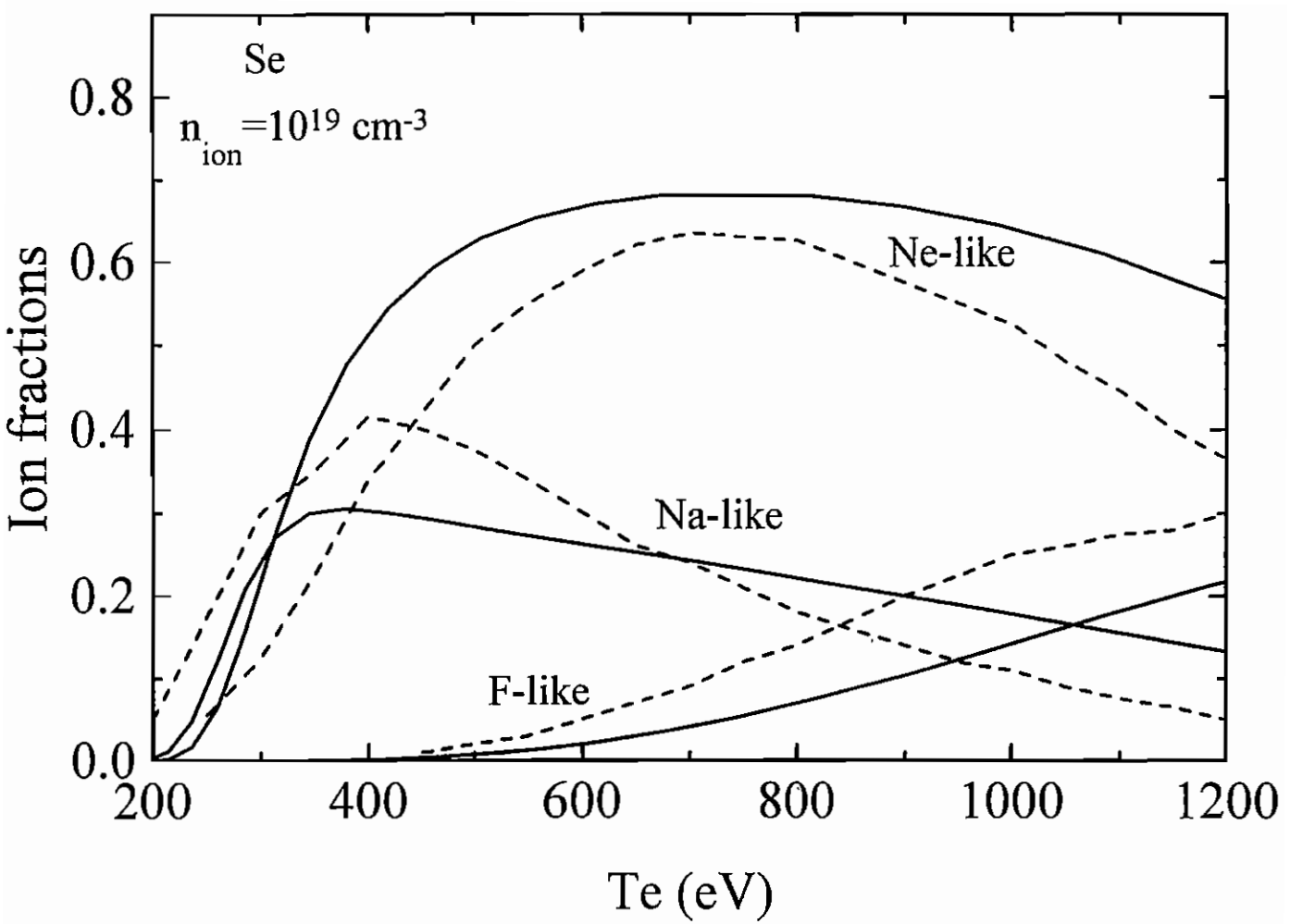


Fig. 2. Steady-state ion fractions of F-like, Ne-like and Na-like selenium at a fixed ion density, as a funtion of electron temperature. The dashed curves are the average level results taken from Osterheld et al[16], while the solid curves are the results from our model.

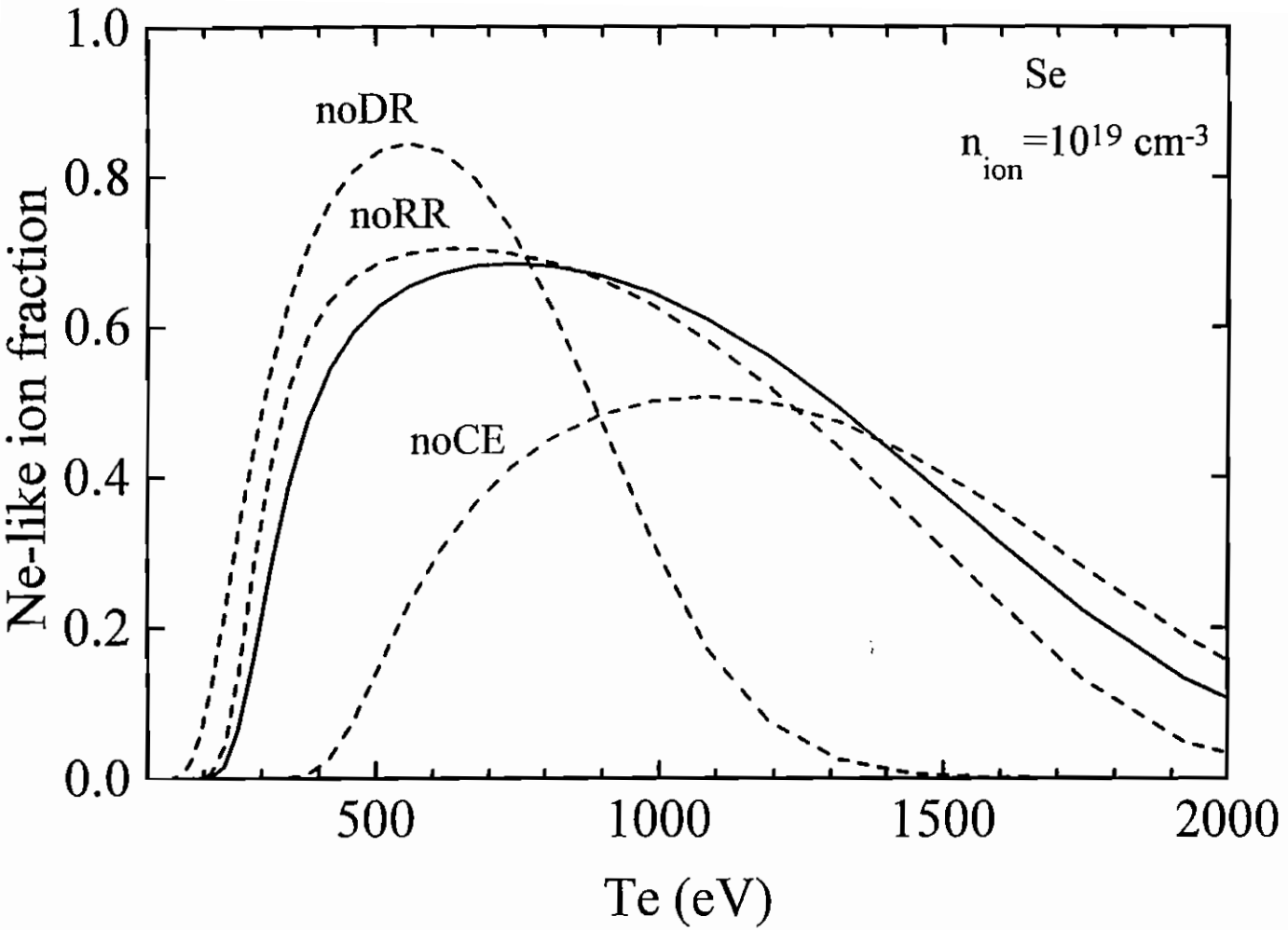


Fig. 3. Effect of switching off either dielectronic recombination (noDR), radiative recombination (noRR) or collisional excitation (noCE) on the Ne-like fraction in selenium plasma at a fixed ion density and as a function of electron temperature. The solid curve includes all atomic processes.

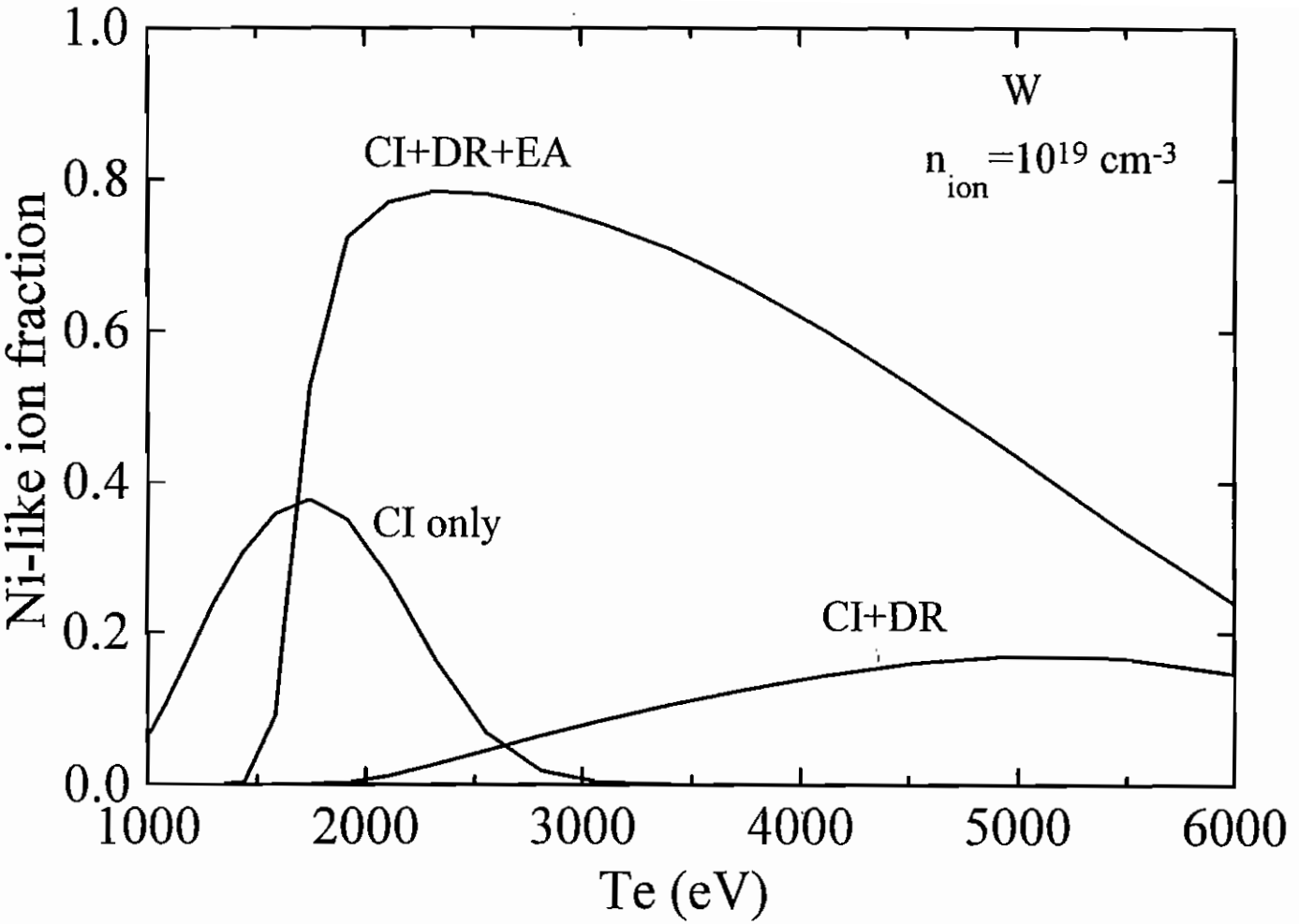


Fig. 4. Dependance of Ni-like ion fraction on collisional ionization (CI) dielectronic recombination (DR) and excitation-autoionization (EA) rates in a tungsten plasma at a fixed ion density and as a function of temperature. The curve with CI only is drastically changed when DR rates are included and when both DR and EA rates are taken into account in addition to CI rates.

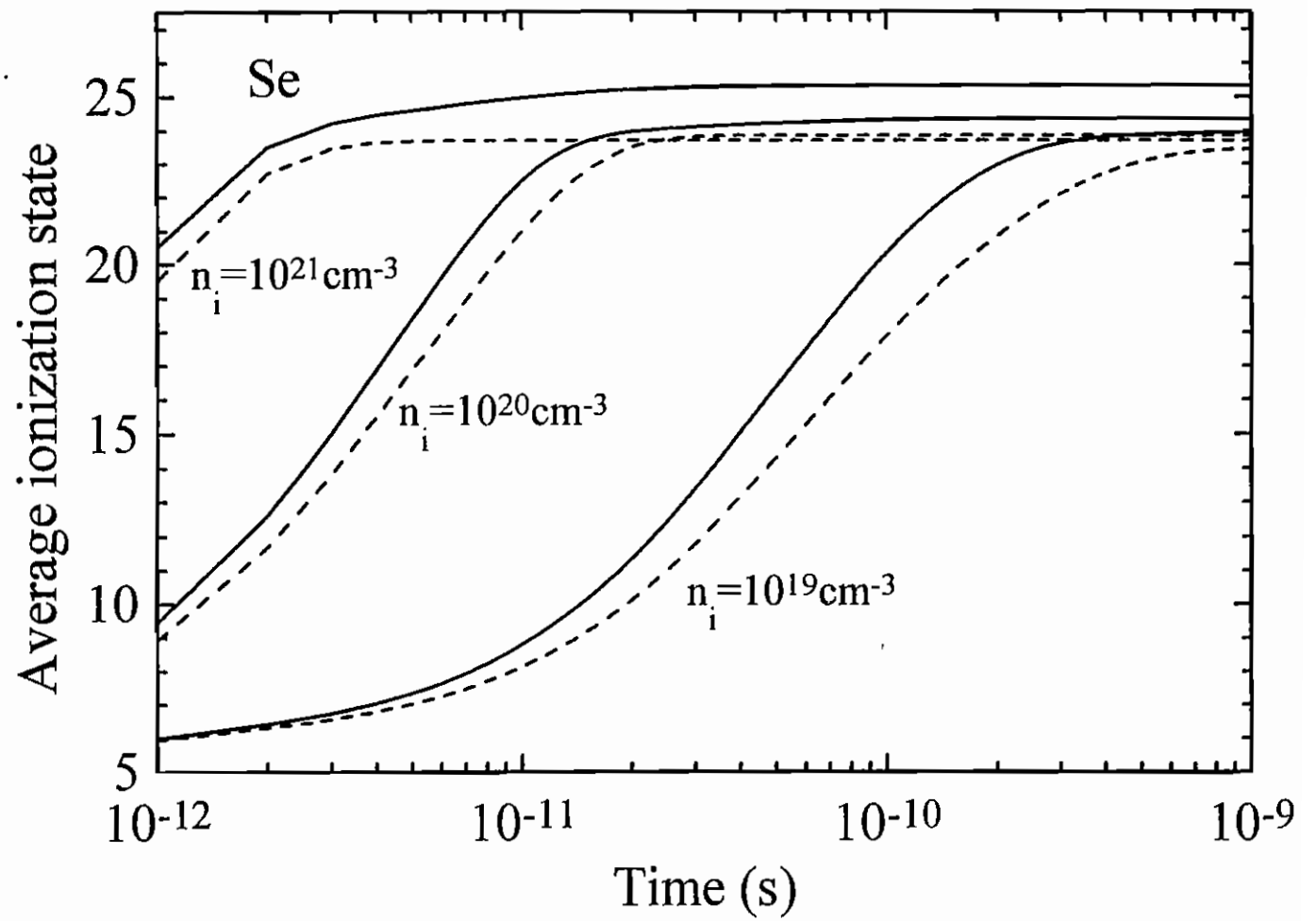


Fig. 5. Time-dependent average charge state of selenium for three ion densities as a function of electron temperature. The dashed curve corresponds to Te = 500 eV and the solid curve to Te = 1000 eV.

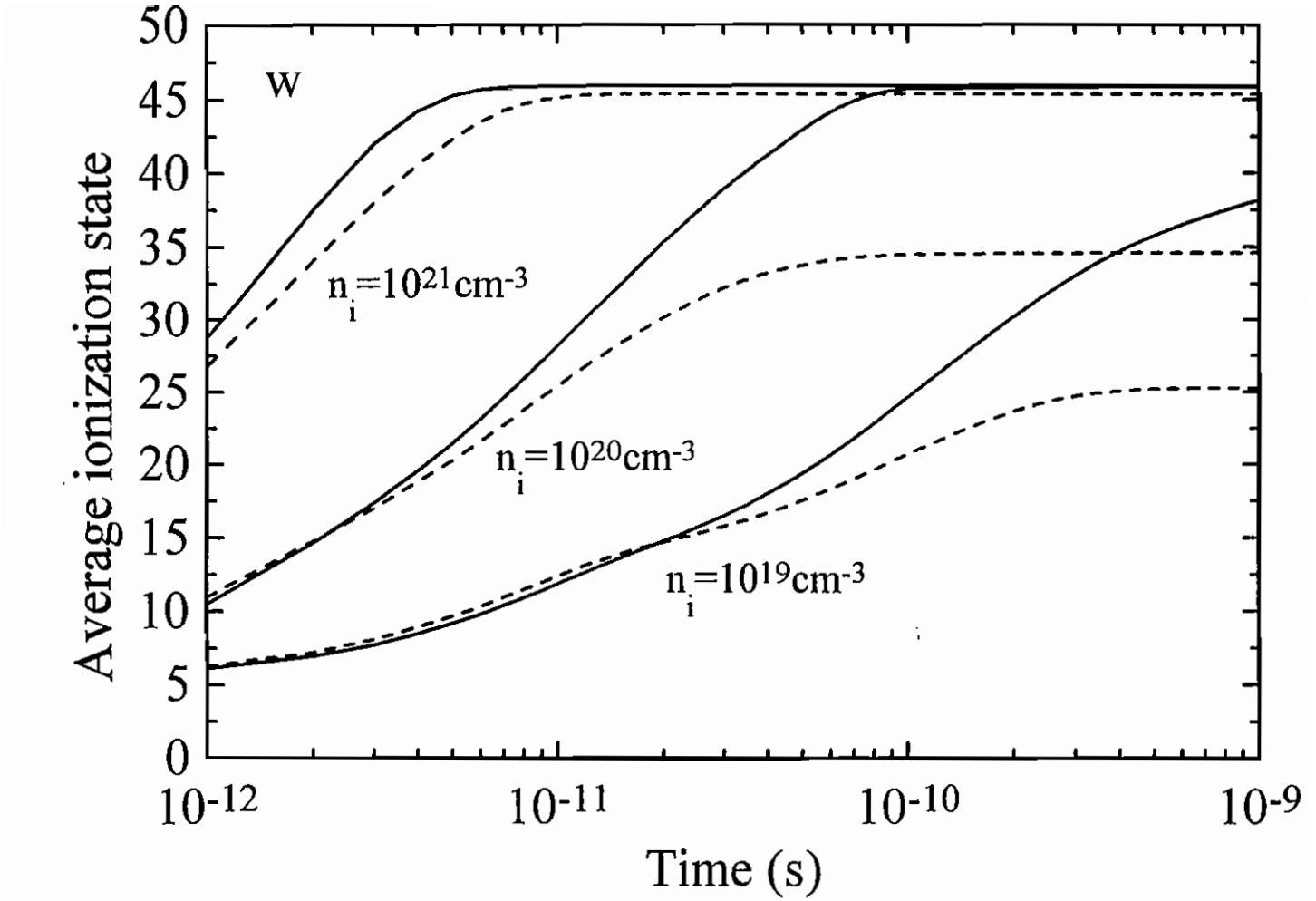


Fig. 6. Time-dependent average charge state of tungsten for three ion densities as a function of electron temperature. The dashed curve corresponds to Te = 1000 eV and the solid curve to Te = 2000 eV.

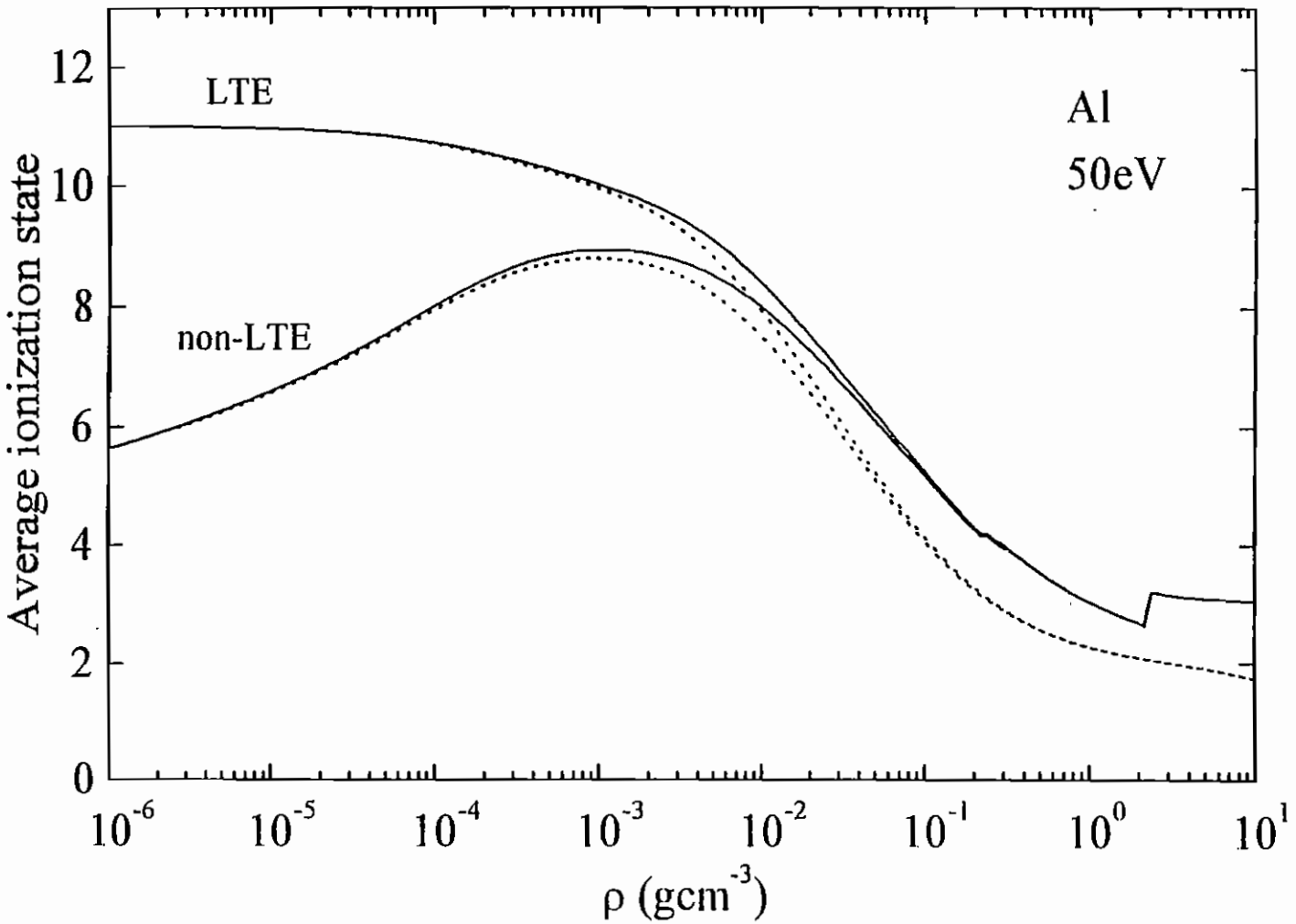


Fig. 7. Comparison of LTE and non-LTE ionization of aluminium at a fixed electron temperature and as a function of density. The calculated results without continuum lowering (dashed) are also shown.

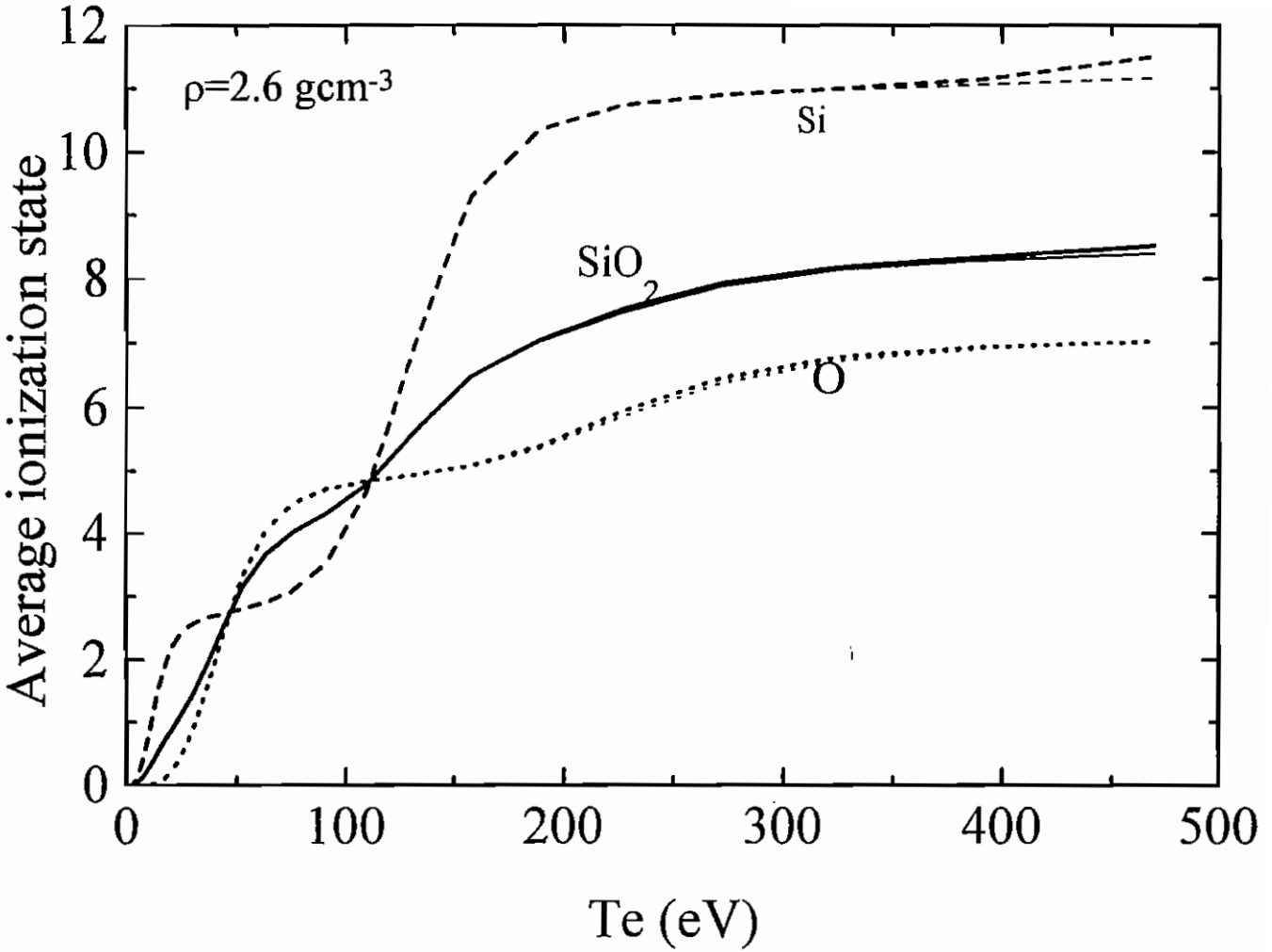


Fig. 8. Calculated average ionization of $SiO_2$ at solid density and as a function of temperature. The partial average ionization of Si and O are shown separately. The thin curves are the result of an LTE calculation.

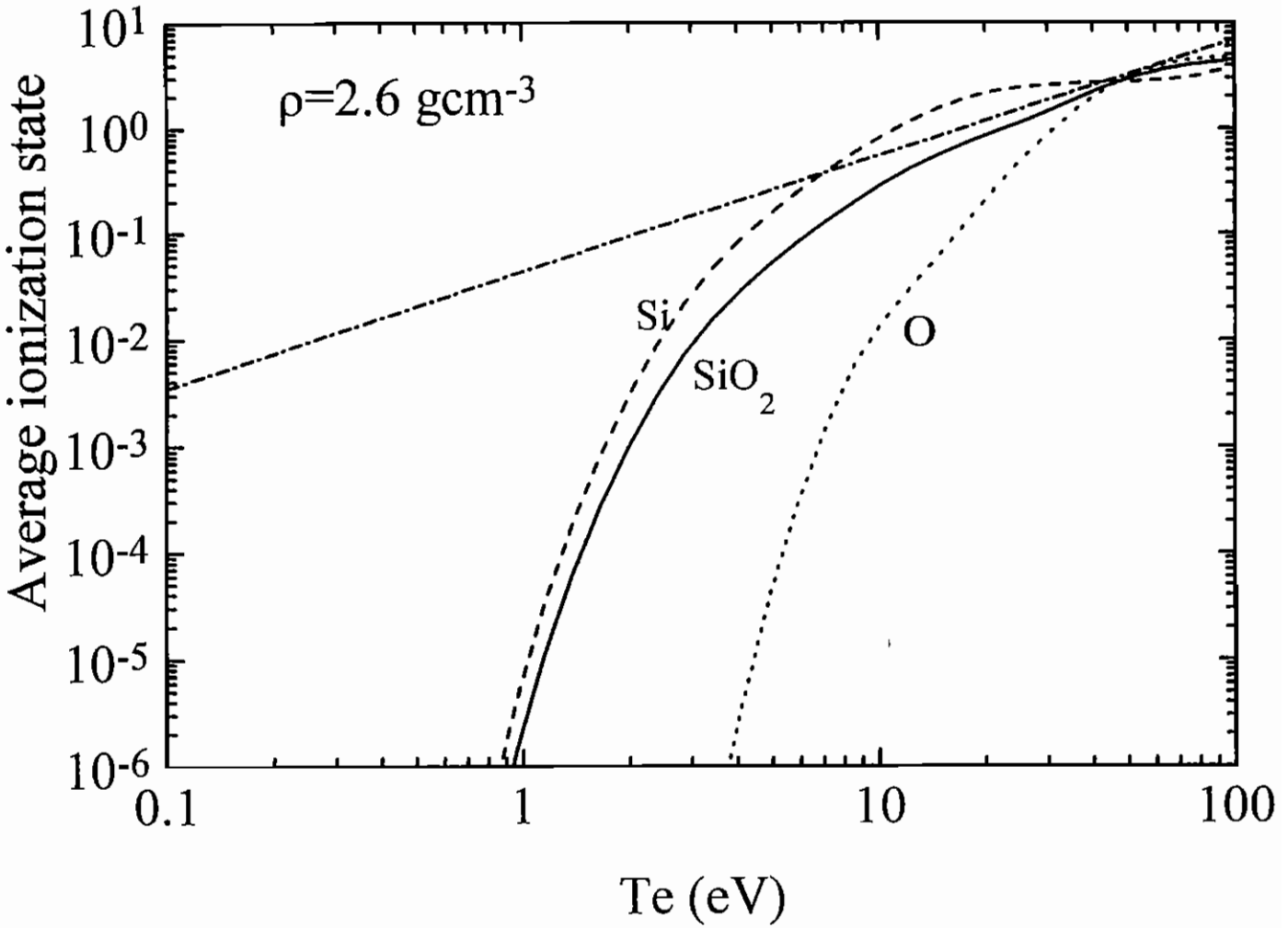


Fig. 9. Calculated average ionization of $SiO_2$ at solid density and as a function of temperature. The partial average ionization of Si and O are shown separately. The dot-dash curve shows the results of the approximate calculation by Vu et al[29].

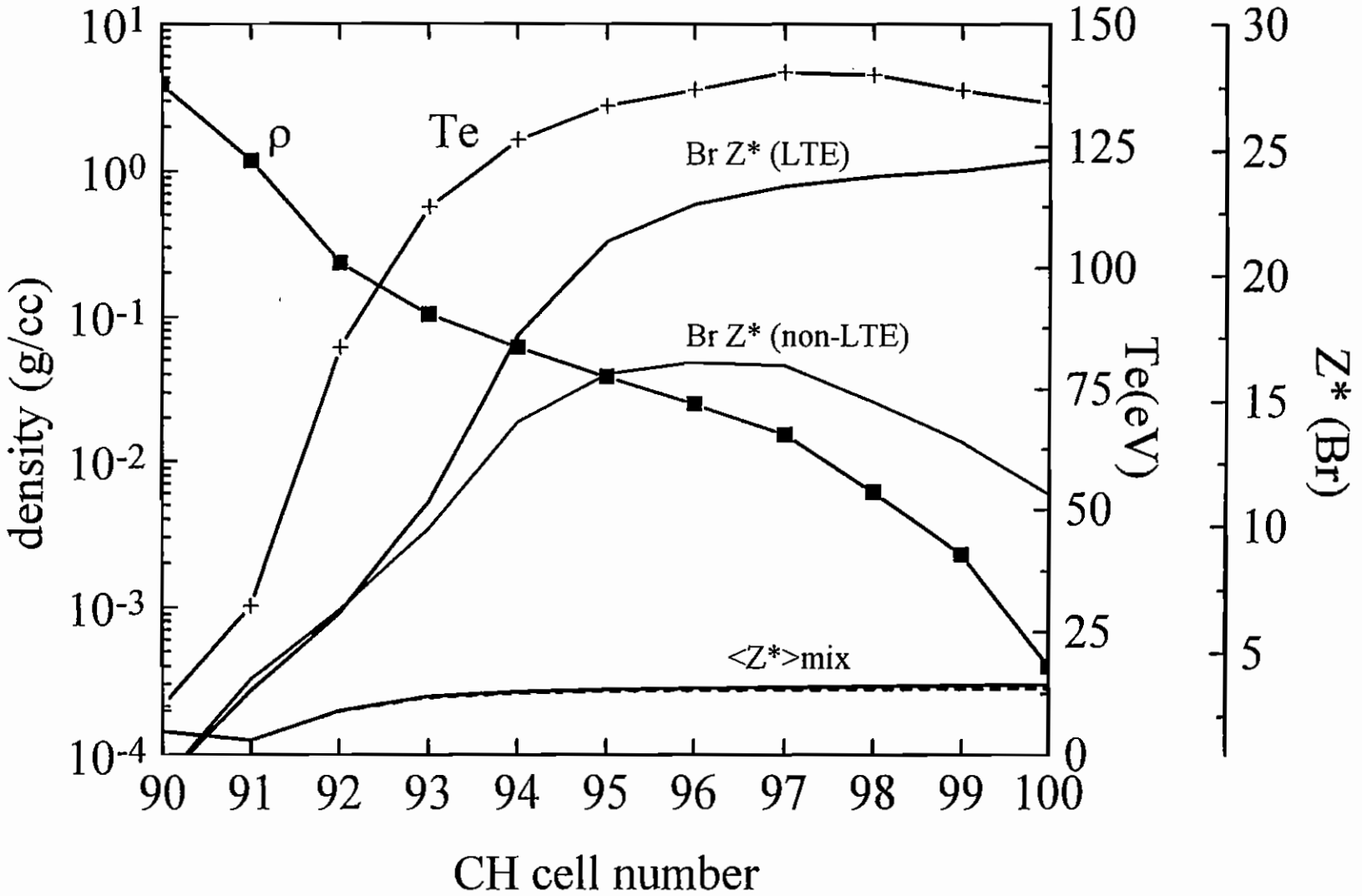


Fig. 10. Density (squares) and electron temperature (+) profiles of a CHBrO ablator shell following irradiation of an indirectly driven ICF capsule. The average ionization state ($< Z^* >$mix) as given by the LTE model (dotted) and non-LTE with no radiation (dashed) are shown. Also shown are the Br ionization state as given by the LTE model and non-LTE with no radiation.

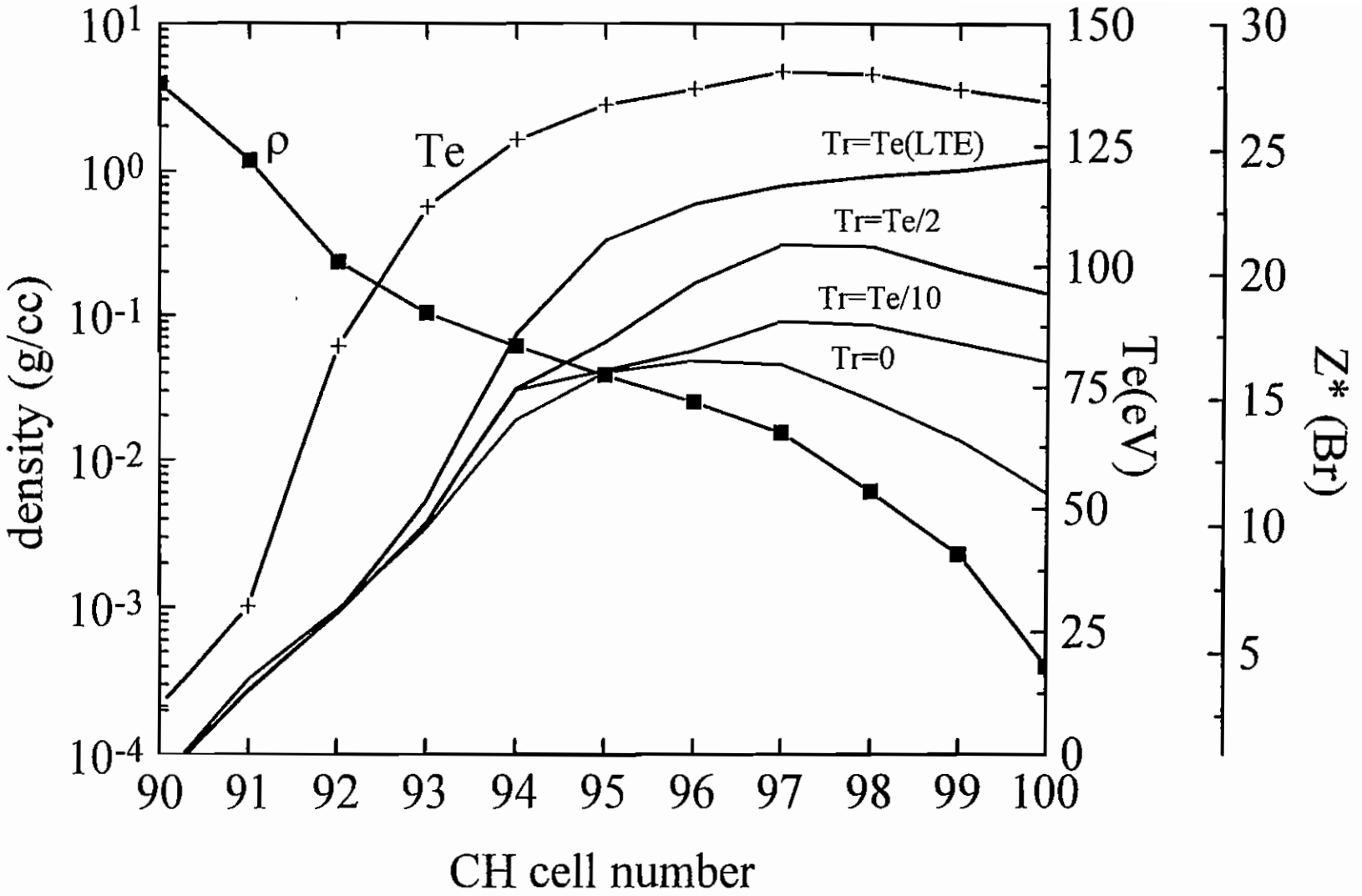


Fig. 11. Density (squares) and electron temperature (+) profiles of a CHBrO ablator shell following irradiation of an indirectly driven ICF capsule. The Br ionization state as given by the non-LTE model with a Planckian radiation field having a temperature (Tr) equal to some fraction of the electron temperature (Te). The case for Tr=Te is similar to the LTE result.

**Table 1:**

| *variable* | *default* | *meaning* |
|---|---|---|
| nspec | 1 | number of species (elements) |
| iatomz(mspec) | 1 | array of atomic numbers |
| atoma(mspec) | 1. | array of atomic masses |
| atomfrac(mspec) | 1. | array of atomic fractions for each species |
| aspomul(mspec) | 1. | array of multipliers for spontaneous emission |
| colemul(mspec) | 1. | array of multipliers for collisional excitation |
| colimul(mspec) | 1. | array of multipliers for collisional ionization |
| radrmul(mspec) | 1. | array of multipliers for radiative recombination |
| diermul(mspec) | 1. | array of multipliers for dielectronic recombination |
| excamul(mspec) | 1. | array of multipliers for excitation/autoionization |
| icolex | 2 | 2: Sampson/Golden formula for col excitation |
| | | 1: Post hydrogenic formula for col excitation |
| zconv | 1.e-8 | convergence criterion |
| zstmin | 1.e-6 | minimum zstart |
| ndens | msize | number of point in density grid |
| rho(msize) | | array of mass densities |
| densi(msize) | | array of ion densities |
| dense(msize) | | array of electron densities |
| tdens | | density step multiplier (dens(id)=dens(id-1)*tdens) |
| ntemp | | number of points in temperature grid |
| tempe(msize) | | array of electron temperatures |
| ttempe | | temperature step multiplier (tempe(it)=tempe(it-1)*ttempe) |
| mode | 1 | 1: use electron densities in steady state cases |
| | | 2: use ion densities in steady state cases |
| | | 3: use mass densities rho in steady state cases |

| | | |
|---|---|---|
| iscl | 1 | 1: include continuum lowering |
| itercl | 1 | 1: perform inner iterations for continuum lowering |
| iterzst | 1 | 1: perform outer iterations for zstar's |
| mitercl | 5 | maximum no of inner iterations |
| miterzst | 200 | maximum number of outer iterations |
| fznew | 0.5 | mixing factor during iteration |
| ngt10 | 0 | 1: include n greater than 10 in LTE solution |
| lte | 0 | 0: perform non-LTE solution |
| | | 1: perform LTE solution |
| trad(msize) | | array of radiation temperatures |
| fradte | | rad temp as a fraction of electron temp (trad(it)=tempe(it)*fradte) |
| iforward | 0 | 0: steady state LTE or NLTE. Grid in density and/or grid in temperatu |
| | | 1: steady state LTE or NLTE from hydro data following namelist |
| | | 2: time-dependent NLTE from hydro data following namelist |
| mode2 | 1 | 1: advance time dependent (iforward=2) using electron densities |
| | | 2: advance time dependent (iforward=2) using ion densities |
| | | 3: advance time dependent (iforward=2) using mass densities |
| nprstep | 1 | number of timesteps between printouts |
| tstep | 1.e-12 | timestep for advancing time in seconds |
| time | | array of times of hydro data |

Table 2: Example output file

```
 Title: example  CH

Number of atomic species in mixture:  2

atomic species: symbol: atomic no: atomic mass: atomic fraction:
          1       C        6         12.000      0.500000
          2       H        1          1.000      0.500000

Multiplier to atomic rates
atomic species: symbol: coli mul: dier mul: radr mul: exca mul: aspo mul: cole mul:
          1       C       1.00       1.00       1.00       1.00       1.00       1.00
          2       H       1.00       1.00       1.00       1.00       1.00       1.00

WARNING iscl = 0 - Inner iterations not needed itercl reset to 0

iscl - Continuum lowering switch 0=off 1=on : 0

itercl - inner iteration  switch 0=off 1=on : 0
mitercl - maximum number of inner iterations :    5

iterzst - outer iteration  switch 0=off 1=on : 1
miterzst - maximum number of outer iterations :  200
ss Number of iterations nitt nitercl          24          1




 Time     Tempel2  Trad2    Densel2  Densil2  Rhol2    Zbar     Zstar1
 0.00E+00 1.00E+00 0.00E+00 3.64E+16 2.41E+17 2.60E-06 1.51E-01 2.68E-01 3.41E-02


 --- T H I S   R E S U L T   I S      F O R ---

 Non-LTE ionisation balance for electron density       (/cc):  3.6365E+16
 Ion density (/cc)  :  2.4088E+17
 Mass density (g/cc):  2.6000E-06
 Electron temperature (eV)         :  1.0000E+00
 Radiation temperature (eV)        :  0.0000E+00

 Average ionisation charge of mixture  :  1.5097E-01      Average ionisation charge squared of mixture  :  3.6451E-02
Atomic species :  1  Ion spectroscopic symbol:  1 Ionz pot: -1.3045E+01
Atomic species :  1  Ion spectroscopic symbol:  2 Ionz pot: -2.7050E+01
Atomic species :  1  Ion spectroscopic symbol:  3 Ionz pot: -4.3476E+01
Atomic species :  1  Ion spectroscopic symbol:  4 Ionz pot: -6.2323E+01
Atomic species :  1  Ion spectroscopic symbol:  5 Ionz pot: -3.9601E+02
Atomic species :  1  Ion spectroscopic symbol:  6 Ionz pot: -4.8978E+02
Atomic species :  2  Ion spectroscopic symbol:  1 Ionz pot: -1.3605E+01

Atomic species :  1 Average ionisation state :  2.6784E-01          Sum of fractions :  1.0000E+00
Partial electron density (/cc):  3.2260E+16 Partial ion density (/cc):  1.2044E+17 Partial mass density (g/cc):  2.4000E-06
Stage States  Total and Partial fractions -----
   1   9  7.3216E-01 7.3180E-01 8.1666E-05 2.7282E-05 2.5187E-05 2.9653E-05 3.5858E-05 4.3056E-05 5.1968E-05 6.2068E-05 0.0000E+00
   2   9  2.6784E-01 2.6784E-01 1.7898E-09 6.7947E-11 2.3488E-11 1.6021E-11 1.4243E-11 1.3984E-11 1.4758E-11 1.6017E-11 0.0000E+00
   3   9  5.3603E-08 5.3603E-08 2.1607E-20 2.6727E-21 1.3885E-21 7.2138E-22 5.2584E-22 4.3421E-22 3.9390E-22 3.7585E-22 0.0000E+00
   4   9  4.3383E-18 4.3383E-18 0.0000E+00 0.0000E+00 0.0000E+00 0.0000E+00 0.0000E+00 0.0000E+00 0.0000E+00 0.0000E+00 0.0000E+00
   5  10  0.0000E+00 0.0000E+00 0.0000E+00 0.0000E+00 0.0000E+00 0.0000E+00 0.0000E+00 0.0000E+00 0.0000E+00 0.0000E+00 0.0000E+00
   6  10  0.0000E+00 0.0000E+00 0.0000E+00 0.0000E+00 0.0000E+00 0.0000E+00 0.0000E+00 0.0000E+00 0.0000E+00 0.0000E+00 0.0000E+00
   7   1  0.0000E+00 0.0000E+00 0.0000E+00 0.0000E+00 0.0000E+00 0.0000E+00 0.0000E+00 0.0000E+00 0.0000E+00 0.0000E+00 0.0000E+00

Atomic species :  2 Average ionisation state :  3.4087E-02          Sum of fractions :  1.0000E+00
Partial electron density (/cc):  4.1055E+15 Partial ion density (/cc):  1.2044E+17 Partial mass density (g/cc):  2.0000E-07
Stage States  Total and Partial fractions -----
   1  10  9.6591E-01 9.6564E-01 5.5832E-05 1.7729E-05 1.5892E-05 1.8084E-05 2.1919E-05 2.6890E-05 3.2831E-05 3.9674E-05 4.7387E-05
   2   1  3.4087E-02 3.4087E-02 0.0000E+00 0.0000E+00 0.0000E+00 0.0000E+00 0.0000E+00 0.0000E+00 0.0000E+00 0.0000E+00 0.0000E+00



td Number of iterations nitt nitercl           9          1
td Number of iterations nitt nitercl           9          1
td Number of iterations nitt nitercl           9          1
td Number of iterations nitt nitercl          10          1
td Number of iterations nitt nitercl          10          1
td Number of iterations nitt nitercl          10          1
td Number of iterations nitt nitercl          10          1
td Number of iterations nitt nitercl          10          1
td Number of iterations nitt nitercl          10          1
td Number of iterations nitt nitercl          10          1




 Time     Tempel2  Trad2    Densel2  Densil2  Rhol2    Zbar     Zstar1
 1.00E-11 1.00E+01 0.00E+00 4.14E+16 2.41E+17 2.60E-06 1.72E-01 3.05E-01 3.86E-02


 --- T H I S   R E S U L T   I S      F O R ---

 Non-LTE ionisation balance for electron density       (/cc):  4.1425E+16
 Ion density (/cc)  :  2.4088E+17
 Mass density (g/cc):  2.6000E-06
 Electron temperature (eV)         :  1.0000E+01
 Radiation temperature (eV)        :  0.0000E+00

 Average ionisation charge of mixture  :  1.7197E-01      Average ionisation charge squared of mixture  :  4.7353E-02
Atomic species :  1  Ion spectroscopic symbol:  1 Ionz pot: -1.3045E+01
Atomic species :  1  Ion spectroscopic symbol:  2 Ionz pot: -2.7050E+01
Atomic species :  1  Ion spectroscopic symbol:  3 Ionz pot: -4.3476E+01
Atomic species :  1  Ion spectroscopic symbol:  4 Ionz pot: -6.2323E+01
Atomic species :  1  Ion spectroscopic symbol:  5 Ionz pot: -3.9601E+02
Atomic species :  1  Ion spectroscopic symbol:  6 Ionz pot: -4.8978E+02
Atomic species :  2  Ion spectroscopic symbol:  1 Ionz pot: -1.3605E+01

Atomic species :  1 Average ionisation state :  3.0531E-01          Sum of fractions :  1.0000E+00
Partial electron density (/cc):  3.6772E+16 Partial ion density (/cc):  1.2044E+17 Partial mass density (g/cc):  2.4000E-06
Stage States  Total and Partial fractions -----
   1   9  6.9507E-01 6.4627E-01 3.5656E-02 5.8699E-03 1.8714E-03 1.1738E-03 9.5889E-04 9.4663E-04 1.0657E-03 1.2537E-03 0.0000E+00
   2   9  3.0456E-01 3.0131E-01 2.4997E-03 3.7876E-04 1.1670E-04 6.4306E-05 4.6385E-05 4.2148E-05 4.5049E-05 5.1896E-05 0.0000E+00
   3   9  3.7560E-04 3.7530E-04 2.5695E-07 2.7253E-08 7.4565E-09 3.5613E-09 2.0660E-09 1.5105E-09 1.3790E-09 1.4697E-09 0.0000E+00
   4   9  8.7456E-09 8.7449E-09 6.2446E-13 4.3133E-14 1.0084E-14 4.3823E-15 2.2521E-15 1.4150E-15 1.1039E-15 1.0599E-15 0.0000E+00
   5  10  5.4894E-15 5.4894E-15 2.0845E-31 4.0028E-34 3.3564E-35 8.2719E-36 4.6490E-36 4.0725E-36 5.3413E-36 7.6385E-36 1.0238E-35
   6  10  1.5874E-29 1.5874E-29 5.1097E-49 2.3532E-51 1.8758E-51 2.0665E-51 3.2581E-51 6.1677E-51 1.1422E-50 1.8988E-50 2.7371E-50
   7   1  4.1094E-44 4.1094E-44 0.0000E+00 0.0000E+00 0.0000E+00 0.0000E+00 0.0000E+00 0.0000E+00 0.0000E+00 0.0000E+00 0.0000E+00

Atomic species :  2 Average ionisation state :  3.8629E-02          Sum of fractions :  1.0000E+00
Partial electron density (/cc):  4.6526E+15 Partial ion density (/cc):  1.2044E+17 Partial mass density (g/cc):  2.0000E-07
Stage States  Total and Partial fractions -----
   1  10  9.6137E-01 9.5723E-01 3.2438E-03 4.9090E-04 1.4452E-04 5.9659E-05 4.0725E-05 3.5043E-05 3.6173E-05 4.0958E-05 4.8272E-05
   2   1  3.8629E-02 3.8629E-02 0.0000E+00 0.0000E+00 0.0000E+00 0.0000E+00 0.0000E+00 0.0000E+00 0.0000E+00 0.0000E+00 0.0000E+00
td Number of iterations nitt nitercl          10          1
td Number of iterations nitt nitercl          10          1
td Number of iterations nitt nitercl          10          1
td Number of iterations nitt nitercl          10          1
td Number of iterations nitt nitercl          11          1
td Number of iterations nitt nitercl          11          1
```